AD-A044 232 MECHANICAL TECHNOLOGY INC LATHAM N Y F/G 13/9
GAS LUBRICATION RESEARCH FOR 1900 F NON-ISOTHERMAL OPERATION.(U)
OCT 68 D WILSON AF 33(615)-3235
UNCLASSIFIED MTI-68TR64 NL

| OF |
AD
A044232

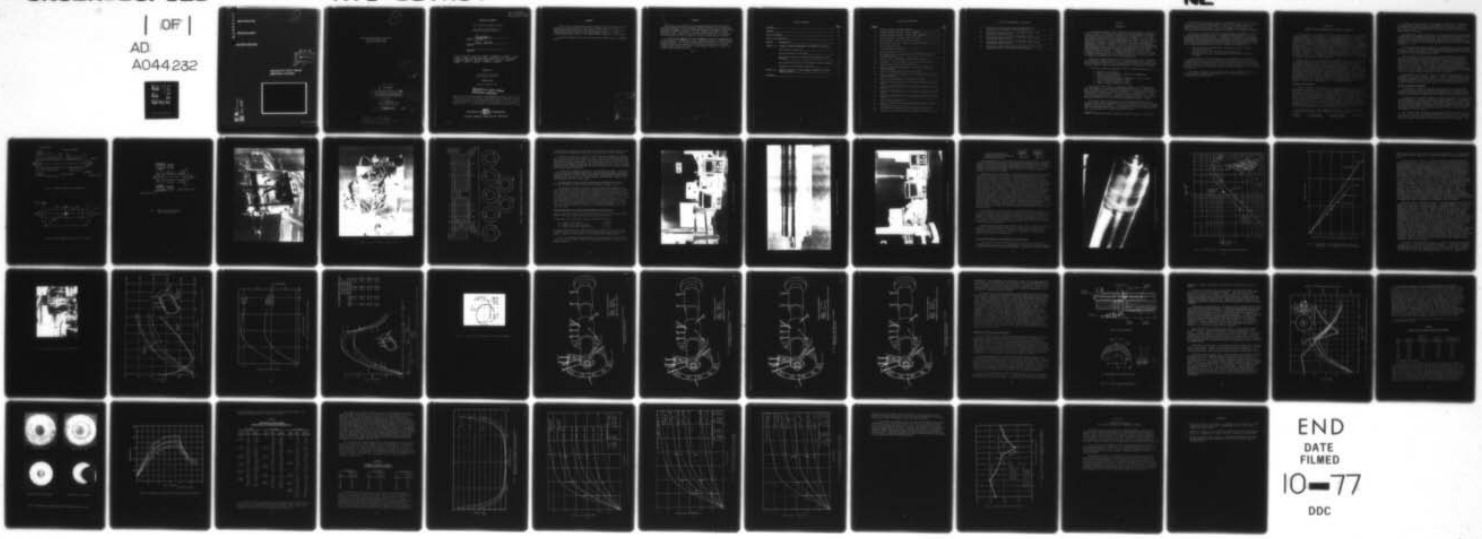

END
DATE FILMED
10-77
DDC

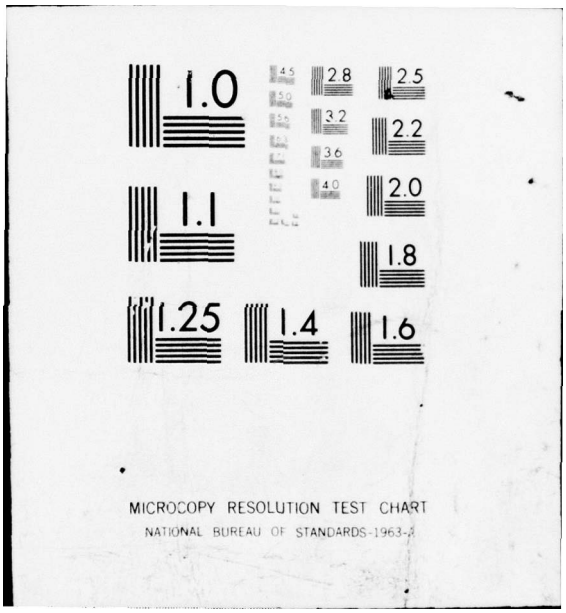
1.0
1.1
1.25
1.4
1.6
1.8
2.0
2.2
2.5
2.8
3.2
3.6
4.0
4.5
5.0
MICROCOPY RESOLUTION TEST CHART
NATIONAL BUREAU OF STANDARDS-1963-A

MECHANICAL

TECHNOLOGY

INCORPORATED

Approved for public release;
distribution unlimited

Mechanical Technology Incorporated
968 Albany-Shaker Road
Latham, New York 12110

MTI-68TR64

Third Semi-Annual Progress Report, no. 3, 1 Mar - 1 Sep 68

GAS LUBRICATION RESEARCH FOR 1900 F NON-ISOTHERMAL OPERATION

by

D. Wilson

Contract AF33(615)-3235

October 7, 1968

52 p.

224 550

NO. MTI-68TR64

DATE: October 7, 1968

TECHNICAL REPORT

Third Semi-Annual Progress Report

Gas Lubrication Research for
1900°F Non-isothermal Operation

D. Wilson

Author -- D. Wilson

Paul Lewis

Approved

Approved

Qualified requesters may obtain copies of this report from DCC. This document is subject to special export controls and each transmittal to foreign governments or foreign nationals may be made only with prior approval of the Air Force Aero Propulsion Laboratory.

Prepared for

United States Air Force
Aero Propulsion Laboratory

Prepared under

Contract AF33(615)-3235

Approved for public release; distribution unlimited

"The work covered by this report was accomplished under Air Force Contract AF33(615)-3235, but this report is being published and distributed prior to Air Force review. The publication of this report, therefore, does not constitute approval by the Air Force of the findings or conclusions contained herein. It is published for the exchange and stimulation of ideas."

MTI
MECHANICAL TECHNOLOGY INCORPORATED
MTI

968 ALBANY - SHAKER ROAD — LATHAM, NEW YORK — PHONE 785-0922

FOREWORD

This report was prepared by Mechanical Technology Incorporated, 968 Albany-Shaker Road, Latham, New York, 12110, under contract number AF33(615)-3235. The work was administered under the direction of the Fuels, Lubrication, and Hazards Branch of the Support Technology Division of the Air Force Aero Propulsion Laboratory with Mr. M. R. Chasman (APFL) acting as project engineer.

The work reported herein covers the period from 1 March 1968 to 1 September 1968.

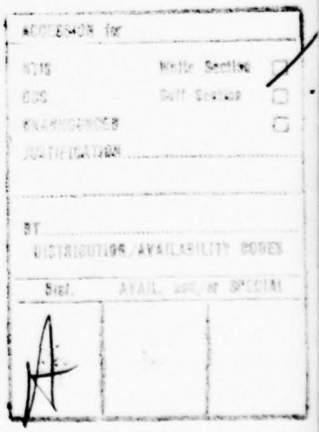

ABSTRACT

Experiments were conducted on herringbone-grooved hydrodynamic journal bearings and spiral-grooved hydrodynamic thrust bearings under non-isothermal operating conditions. Journal bearing performance was determined under thermal gradients to 120°F/inch axially, 180°F/inch radially, and 133°F/π radians circumferentially. Under these conditions, bearing characteristics could be predicted within ten percent using the effective average bearing clearance.

A double-acting hydrodynamic thrust bearing was evaluated with thermally induced gradients to 67°F/inch radially, 240°F/inch axially and 60°F/π radians circumferentially. The effective bearing axial clearance after accounting for bearing distortions as determined from statically measured axial end play readings agreed within five percent of the clearance required to predict the measured dynamic characteristics.

TABLE OF CONTENTS

LIST OF ILLUSTRATIONS

SECTION I

INTRODUCTION

As engineering advances improve materials and machine design techniques, there is a trend for turbomachinery operation at higher speeds and temperatures. To keep abreast with this trend, a need exists for improvements in the rotor bearing and lubrication support systems for this equipment. The use of gas as the lubricant medium offers obvious advantages over commonly used liquid and grease type lubricants. Previous experimental work (1)* has demonstrated the feasibility of gas bearing operation in an inert isothermal environment at temperatures to 1400°F. However, in order to apply gas lubricated bearings to high temperature applications which typically impose oxidizing environments and thermal gradients, additional information regarding materials and bearing distortion effects is required. Although consideration could be given to isothermal bearing operation, the limitations imposed on turbomachinery design to eliminate thermal gradients in the bearing region are considered too great to consider this approach practical in most applications.

The present program was initiated to investigate these areas. Basically, the program has a twofold purpose, i.e., to investigate materials suitable for use in bearings and construction to temperatures of 1900°F and to determine gas bearing limitations under non-isothermal conditions to temperatures of 1900°F.

A five step program was conducted to select suitable bearing materials; i.e.,

1. Review of base materials.
2. Review of surface coatings suitable for high-speed rubs and start-stop operation.
3. Thermal dimensional stability evaluations of base materials in an oxidizing environment to 1400°F.
4. Static coating evaluations to 1900°F.
5. Dynamic coating evaluations to 1400°F.

As a result of the material investigation program, a nickel base super alloy (Hastelloy X) was selected as the bearing base material. Although this alloy was selected as one of the best materials for the experimental conditions, there was still evidence of dimensional instability at temperatures of 1400°F of the order of 1×10^{-4} inches. It was felt that gas bearings may be capable of short term operation within the dimensional changes encountered. No suitable material was found for use in an oxidizing environment at 1900°F, however.

The surface coating selected was a nickel-chrome bonded chrome carbide sprayed surface on the rotating member and a self-bonded aluminum oxide sprayed coating on the stationary member. This combination was not impervious to damage under the conditions imposed, but was representative of the best combination of known available materials for applications above 1000°F.

---

*Numbers in parenthesis refer to references listed at the end of this report.

The results of the material studies are summarized in Refs. (2) and (3) and indicate that presently available materials and coatings appear suitable for short term operation but further development is required for prolonged operation at 1400°F in oxidizing environment. There do not appear to be any present day materials suitable for gas bearing operation at 1900°F in an oxidizing atmosphere.

In order to investigate limitations of gas bearings at temperatures of 1400°F, a plain cylindrical hydrostatic and a herringbone-grooved hydrodynamic journal bearing were selected for evaluation. In addition, a hydrostatic thrust bearing and spiral-groove hydrodynamic thrust bearing were also utilized for experimental evaluations. The primary concern in bearing design under non-isothermal operation is the induced bearing distortions that can result from thermal gradients. Therefore, a three-phase program was outlined for bearing investigations, i.e.:

1. Bearing operation and performance determination under mechanically distorted conditions.
2. Bearing operation under thermally distorted conditions.
3. Bearing operation under non-isothermal conditions and temperatures to 1400°F.

Under mechanical distortions, generally both hydrostatic and hydrodynamic bearings tend to average out the variations in bearing clearance and function as a bearing with this average clearance. Similar results were obtained by thermally inducing distortions in hydrostatic journal and thrust bearings. The experimental results of the mechanical and thermal induced distortions are detailed in references (2) and (3).

This report summarizes the experimental work conducted during the period of 1 March through 1 September 1968 concerned with thermally induced distortions on hydrodynamic bearing performance.

SECTION II

THERMALLY INDUCED HYDRODYNAMIC GAS BEARING DISTORTIONS

In the operation of turbomachinery at high ambient temperatures, considerable design penalties are encountered if it is necessary to operate the bearings in an isothermal condition. The existence of thermal gradients on the other hand introduces distortions of the bearing reducing bearing capabilities. In order to determine the influence of the distortions on bearing performance, such things as taper, out-of-roundness and misalignment were mechanically induced in the bearings. In actual machines, it is more probable that bearing distortions would result from thermal effects rather than machanical loading. To investigate the effects of thermally induced distortions on hydrodynamic bearing performance, an experimental rig that was capable of inducing thermal gradients in the bearing region was utilized. Comparison of performance with and without gradients introduced should provide the basis for a recommendation on how to handle the design of hydrodynamic gas bearings operating with thermal gradients.

Direct control on the degree and type of distortion was possible during the mechanically induced distortion phase of the program. This, however, was not the case when thermal gradients were induced around the bearing region. It was anticipated, therefore, that the bearing would be subjected to a combination of distortions simultaneously which could not be readily separated. Actual measurements of the distorted condition of both shaft and bore while at temperature were attempted without too much success. The primary difficulty arises from the fact that thermal transients induce considerable drifting of electronic gages while air gages tend to cool the parts. Therefore, the thermocouples located around the bearing region were used to provide the indication of the degree of distortion. Despite this difficulty, meaningful results were obtained which will assist the designer of bearings for high temperature non-isothermal operation.

Test Rig (Non-Isothermal)

Actual turbomachines usually consist of a bearing supported rotor with a hot turbine wheel attached to one end and a cold output shaft at the other. Such a configuration frequently results in thermal gradients at all bearing locations with particularly high ones at the hot end bearings. The test rig used for this program is designed to simulate the configuration of the turbomachine. At one end of the rotor a circumferential row of heaters surrounds a thrust and journal bearing simulating the hot end of a turbomachine. At the other end of the rotor is a second journal bearing and a small impulse turbine. Expansion of cold gas through the turbine acts as a small heat sink and aids in maintaining an axial gradient along the test rotor. All rig components are made from Hastelloy X and were specially heat treated to assure good dimensional stability.

The test rig shown in block diagram form in Figure 1 was used during all thermal gradients testing. Major components of this test rig are:

1. Rotor
2. Turbine
3. Thrust Runner
4. Thrust Bearings
5. Journal Bearings
6. Position Sensors
7. Speed Pickup

The rotor configuration used for all gradient tests is shown in Figure 2. This rotor weighs 5.75 lbs., has a polar moment of inertia of $I_p = 5.89 \times 10^{-3}$ in-lb-sec^2 and a transverse moment of inertia about its center of gravity of $I_{xy} = 0.122$ in-lb-sec^2. A drive turbine is mounted on one end of the rotor, a thrust runner on the other.

The hydrodynamic thrust bearing was of the inward pumping spiral groove type. A double-acting configuration was utilized with a stationary thrust plate located on either side of the rotating thrust disk. End play was controlled by the spacer located between the two stationary thrust plates as schematically depicted on Figure 1. A 2.625 inch thrust runner diameter was used with an outer to inner radius ratio of 1.5.

The two journal bearings are identical in design and are 1.5 inches in diameter by 1.5 inches long. Both contain fully grooved herringbone configuration in the journal region for stability. The details of the bearing design are discussed in the section containing experimental results.

Heat is applied to the test rig in two zones, one located at the thrust bearing, and the other at the journal bearing nearest the thrust bearing. The heat source at each area consists of six 200 watt heater cartridges, equally spaced circumferentially within the heater zone. The position of each heater zone is shown in Figure 3. Heater control is provided by nine autotransformers; three used to control three pairs of thrust heaters and six to individually control the journal heaters. In the event sufficient temperature levels cannot be achieved, the gas supply to the bearing can be directed through a gas preheater. Details of the gas preheater design can be found in Reference 1.

An assembled view of the test rig prior to insertion of thermocouples and attachment of gas lines is shown in Figure 4. Figure 5 shows the manner in which the heater cartridges are inserted in the rig. To aid in determining the extent of thermal gradient imposed on the test rig, many thermocouples were placed in strategic locations in the test rig. Figure 6 shows where these locations are.

Bearing Performance Evaluations

To establish the effect of thermally induced distortions on hydrodynamic bearing performance, a series of controlled experiments were performed. Tests both with and without thermal gradients were conducted and a record was kept of several basic performance factors such as stiffness, and whirl threshold speeds.

Evaluations of the journal bearings were conducted separately from the thrust bearing experiments. Therefore, hydrostatic thrust bearings were installed for the hydrodynamic journal evaluations. During hydrodynamic thrust bearing experiments, hydrostatic journal bearings were installed. Operation, therefore, could be started on the hydrostatic bearings and the hydrodynamic could be loaded after attaining operating speed. This method of operation minimized starting torque requirements of the air turbine.

The procedure used in making the journal bearing calibration test was as follows. With the spin axis of the rotor oriented vertically, the drive turbine was pressurized and the rotor brought slowly to a preselected speed. When this speed was reached, the entire test rig was tilted toward the horizontal. At

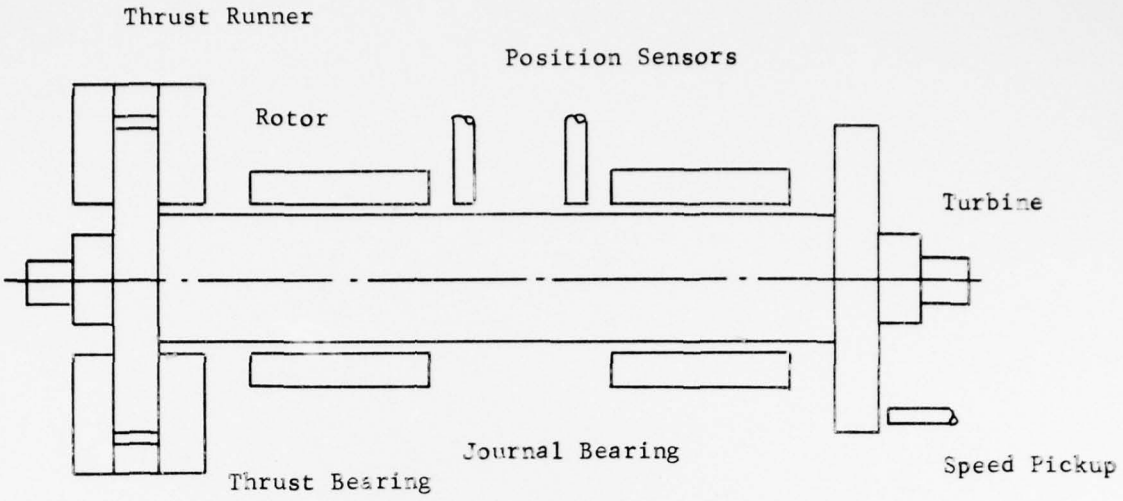

Fig. 1 Thermal Gradient Test Rig Schematic

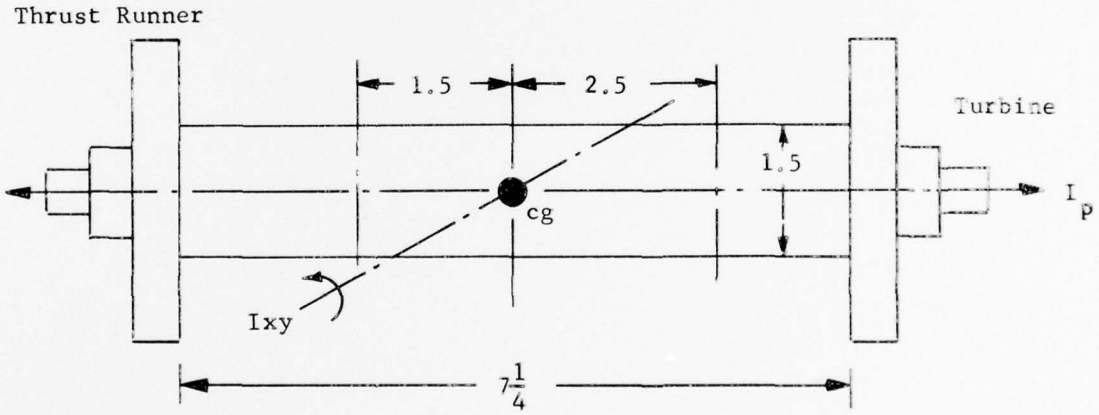

Fig. 2 Thermal Gradient Test Rig - Rotor Schematic

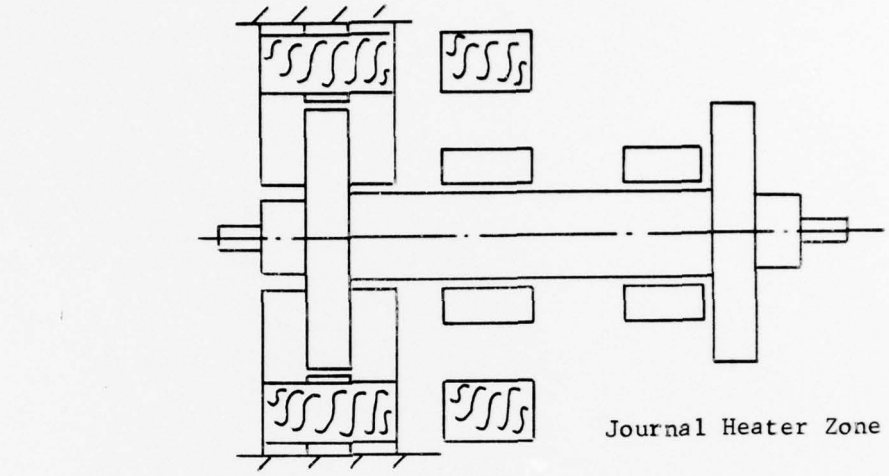

Fig. 3 Thermal Gradient Test Rig
Heater Zones Schematic

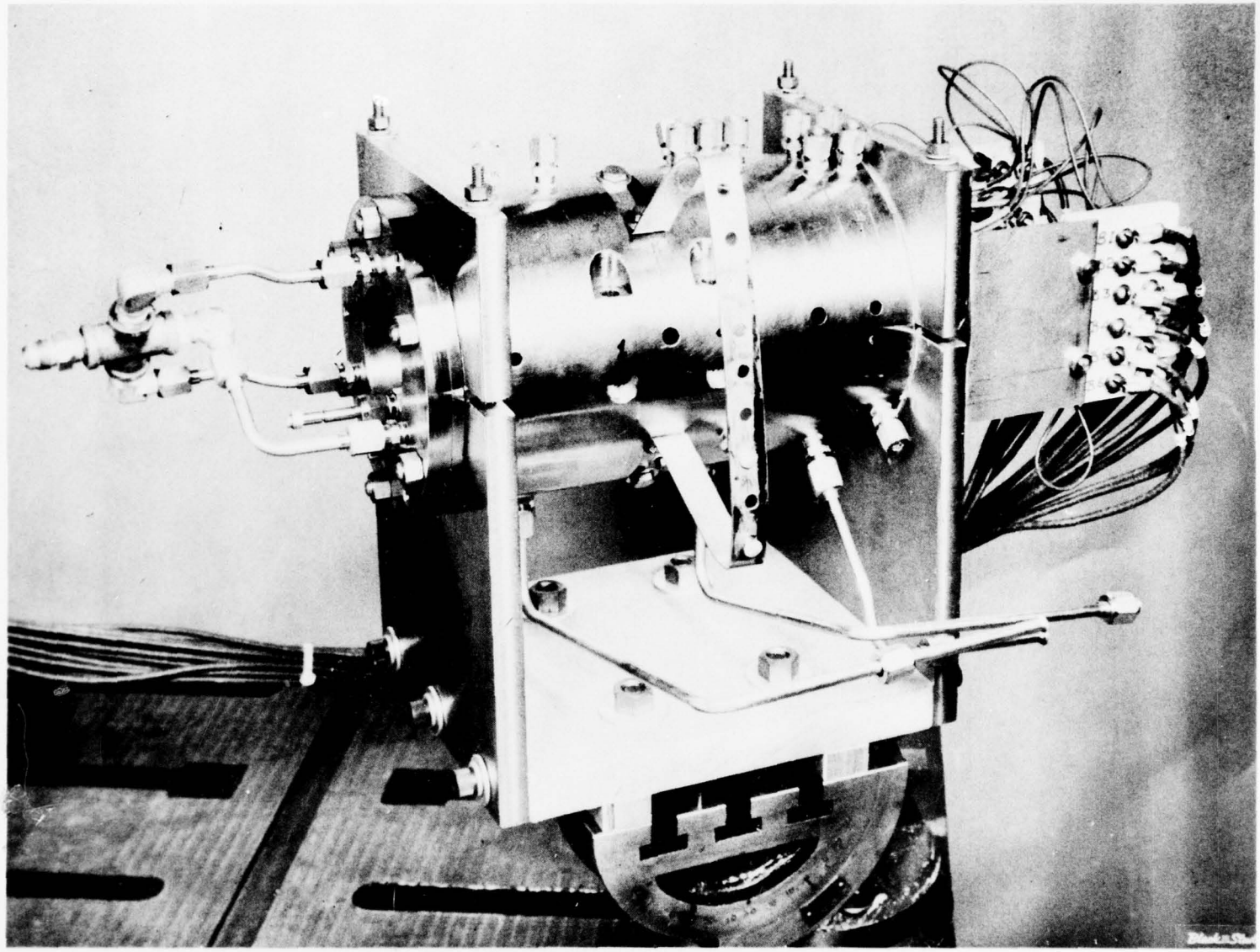

Fig. 4 Partial Assembly-Thermal Gradient Test Rig

MTI-5393

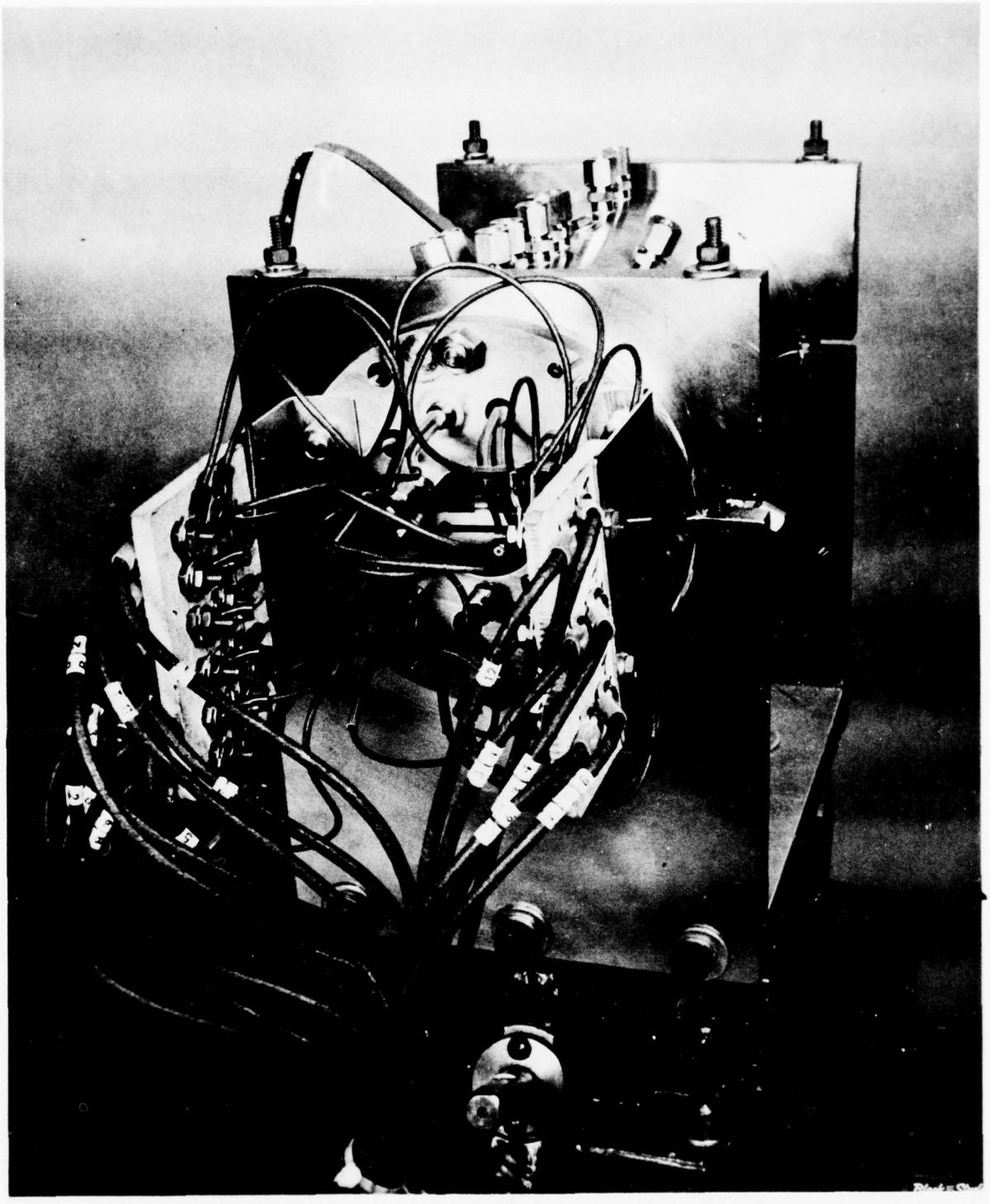

Fig. 5 Heater Positions - Thermal Gradient Test Rig

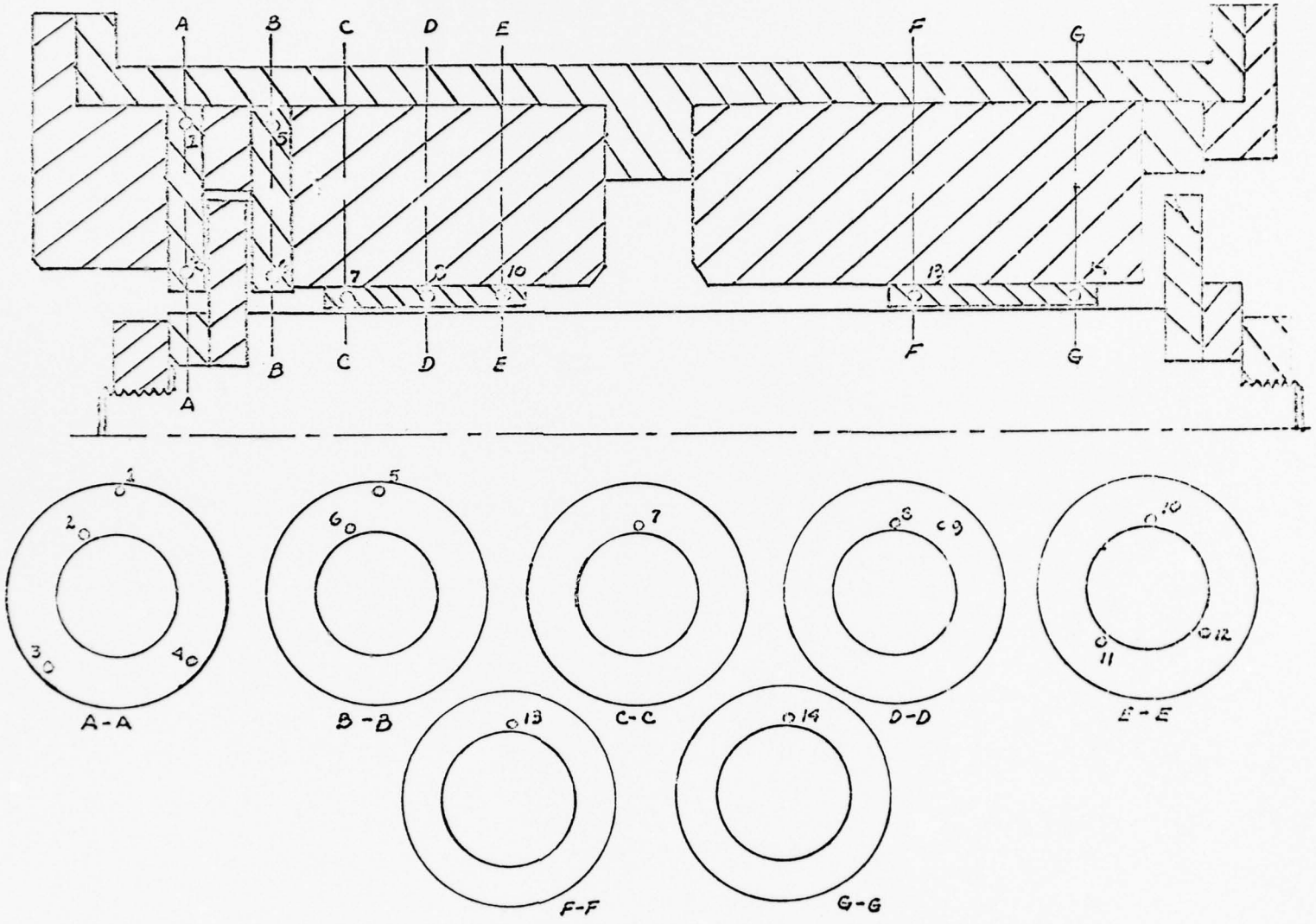

Fig. 6 Thermocouple Locations - Thermal Gradient Test Rig

MTI-5390

several angular increments corresponding to fixed amounts of radial bearing load, the test rig was rotated about the rotor's spin axis in 45 degree increments.

At each tilt position, as the test rig was rotated, a sequential photograph was taken of the rotor orbit display on a CRO. The result of these photographs was an eccentricity circle at each of the fixed radial loads corresponding to the particular tilt angle photographed. The increase in the eccentricity circle diameter with increasing tilt angle defined the stiffness of the bearings. To obtain stiffness data at additional speeds, the rig was returned to the vertical position and the test procedure repeated.

In addition to stiffness information, the calibration procedure included the collection of whirl threshold speed data. Because the hydrodynamic test series would be conducted at only one bearing clearance, the whirl speed would be determined only as a function of two rotor positions; vertical with no journal load and horizontal with full journal loads.

As previously indicated, during evaluations of the hydrodynamic thrust bearing, hydrostatic journal bearings were utilized to support the rotor.

The procedure followed to determine thrust bearing characteristics was to start operation in the shaft horizontal increasing speed to 10,000 RPM. The rig was tilted 5 degrees thrust end down to load one face of the thrust system. At this condition a reading was taken from a capacitive probe sensing shaft end play. This reading was utilized as the initial starting point for the test. The rig was then tilted to horizontal and the axial movement of the shaft recorded. Loads were then applied on the reverse thrust bearing in varying increments and the axial shaft displacement recorded. The reason for loading on both thrust faces was to eliminate any unbalance load errors at the shaft horizontal, zero load position. This procedure was repeated at 15,000 and 20,000 RPM at room temperature conditions.

Experimental Results of Undistorted Herringbone Journal Bearings

Prior to rig operation the journal bearings and rotor were dimensionally checked. Figure 7 shows the inspection setup used to measure the rotor.

Measurements taken during this inspection showed the following:

A. Average rotor diameter - 1.49839
B. Average rotor out-of-roundness - 50 μ in.
C. Average rotor taper (Bearing area) - 50 μ in.

An enlarged photograph of the herringbone pattern etched on the rotor at each bearing location is shown in Figure 8. The helix angle of the grooves is 32.8 degrees. Each of the 36 grooves is 0.035 inch wide and 0.0006 inch deep.

The journal bearings were measured using a setup similar to the one used to measure the rotor. Figure 9 shows a bearing during inspection. Results of the bearing inspection:

MTI-5874

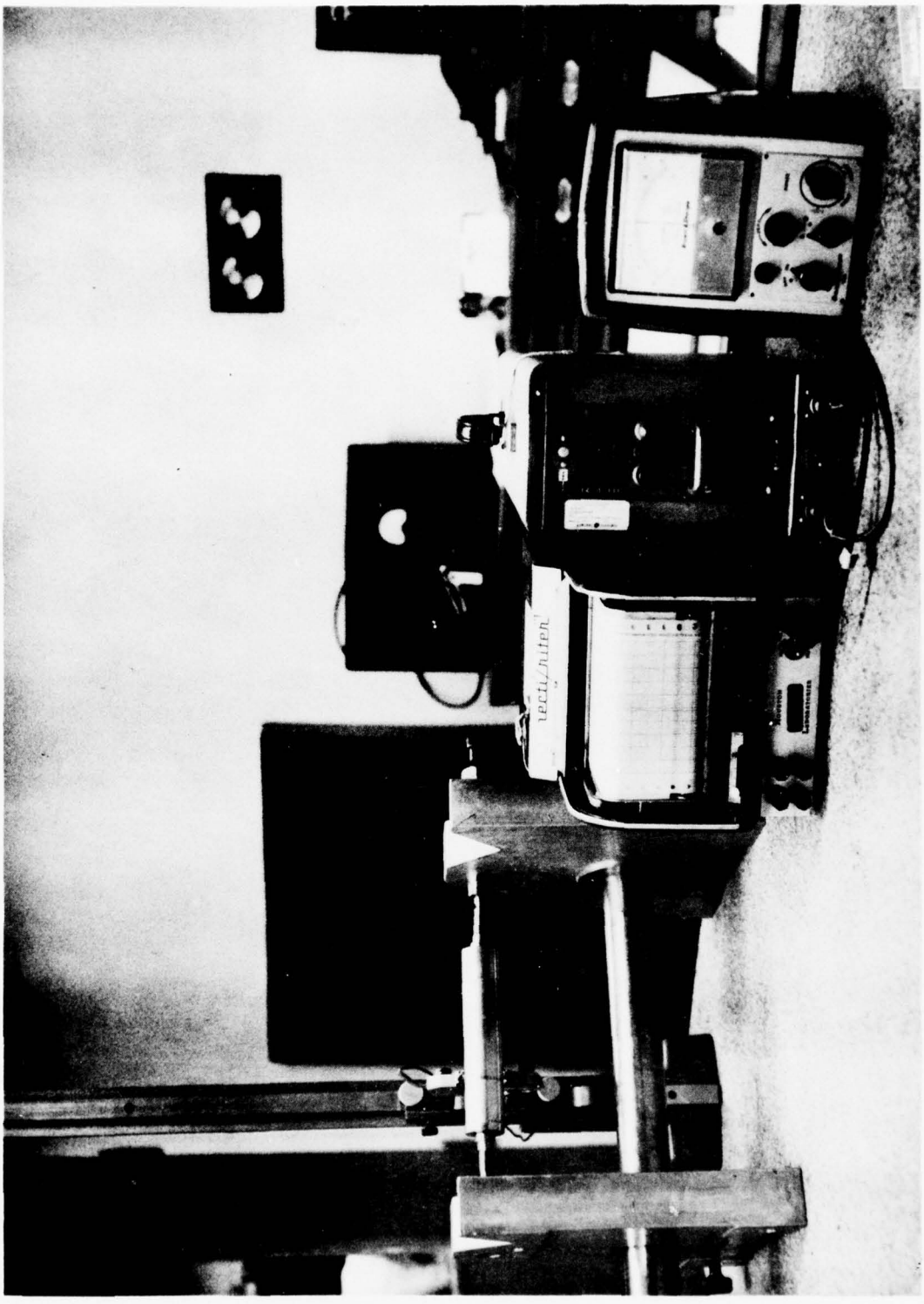

Fig. 7 Shaft Inspection Setup

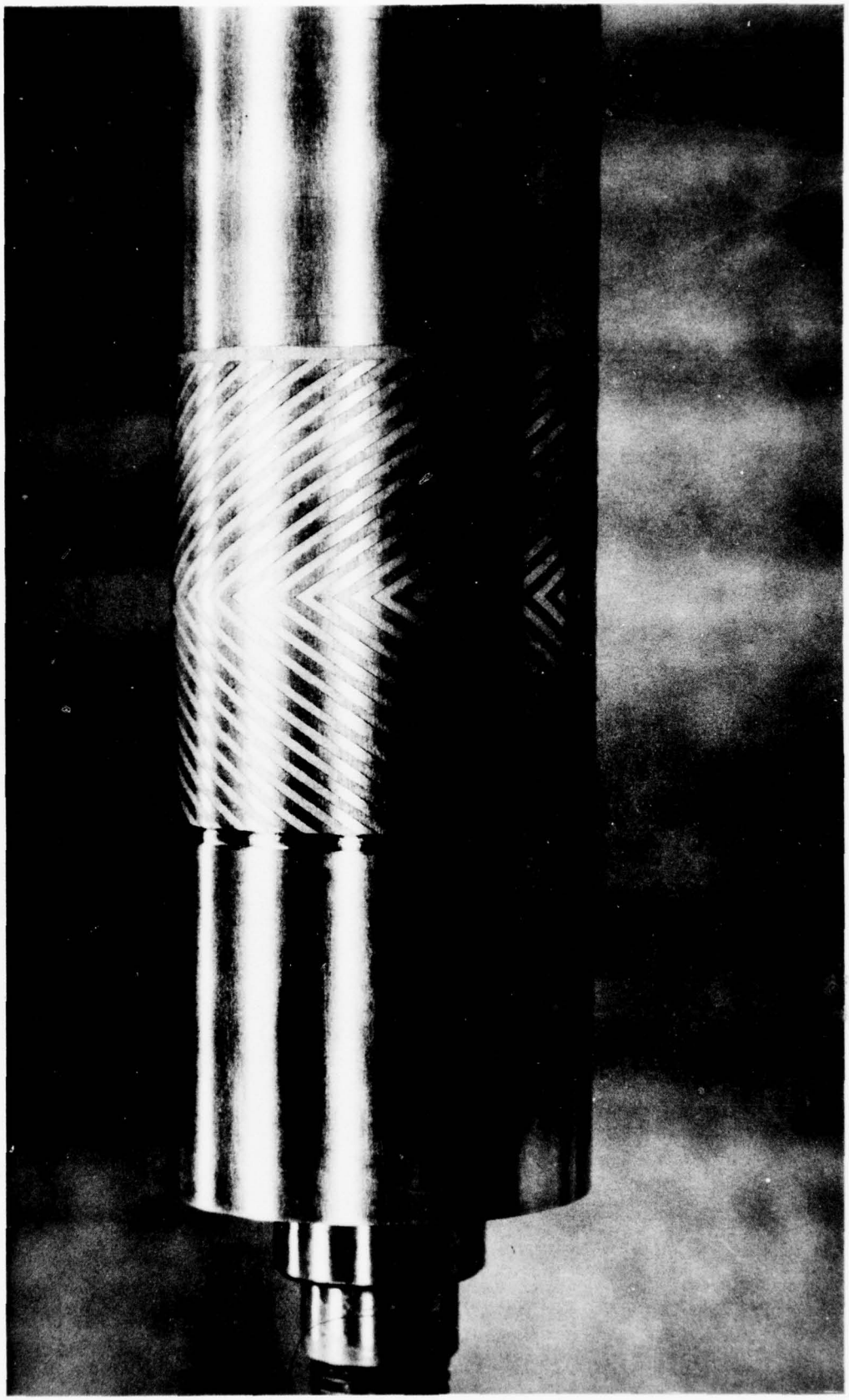

MTI-5392

Fig. 8 A Herringbone-Grooved Pattern

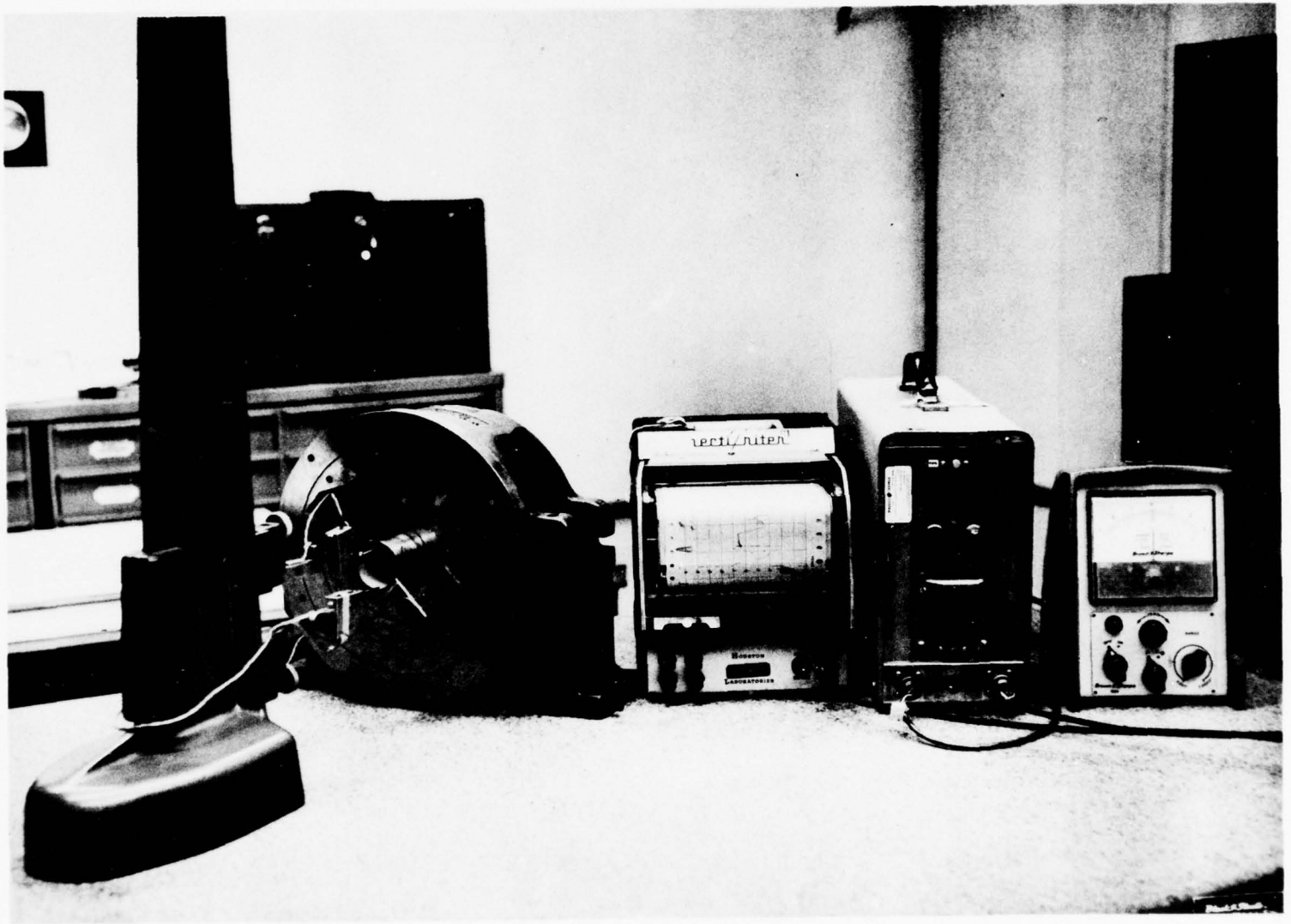

Fig. 9 Bearing Inspection Setup

	Turbine End Bearing	Thrust End Bearing
Average Bearing Diameter	1.499323 in.	1.499548 in.
Average Bearing Out-of-Roundness	150 μ in.	63 μ in.
Average Bearing Taper	100 μ in.	105 μ in.

Following inspection, the bearings and the rotor were installed in the test rig for a performance calibration. This calibration was made under isothermal conditions and was directed toward determination of stiffness and whirl threshold speeds at several load conditions. The purpose of the calibration test is to establish the performance characteristics to which all the non-isothermal performance tests are to be compared.

During the initial calibration, a bearing seizure was encountered at 32,000 rpm and was typified by the transfer of aluminum oxide from the bore of the bearing to the surface of the journal. The failure was attributed to debris entering the bearing during operation causing a localized loss in bearing clearance. The foreign matter was assumed to be generated from the high temperature seals around the capacitive probes which tend to flake off particles when adjusting the probes. Only twenty-five percent of the bearing was damaged on the inboard end as shown on Figure 10. An attempt was made to clean and continue to use the bearing with a partial loss in load capacity after correcting the probe seal condition. However, flaking of aluminum oxide particles from the damaged portion of the bearing bore induced two more bearing failures at 19,700 and 40,850 rpm respectively. The second failure caused sufficient damage to prevent any further operation. It was apparent that the initial failure should have been completely repaired to avoid the latter two seizures. At this point, the shaft journal was ground down and rebuilt by metal spraying and the herringbone pattern photo etched on the shaft. The bearing bore was ground and resprayed with aluminum oxide. The journal was finished straight within 75 microinches per inch and round radially to within 25 microinches with an average radial clearance of 800 microinches.

After completion of bearing repairs, bearing calibration was conducted by initially tilting the rig to the shaft vertical condition (zero eccentricity) and the threshold speed of whirl instability determined. The results are plotted on Figure 11, compared to the experimental results obtained using the mechanical distortion rig described in reference 3. As noted, the threshold speed compared very closely to the previously obtained experimental data. The actual measured threshold speed was 12,500 rpm.

Operating speed was reduced to 12,000 rpm and the load displacement characteristics of the bearing were rechecked by tilting the rig toward the shaft horizontal. This was repeated at 10,000 rpm. The results, compared to predicted performance, are plotted on Figure 12. Once again, the experimental compared very closely to the predicted.

Non-isothermal Operation of Hydrodynamic Journal Bearings

Upon completion of the initial calibration, the rig was returned to the vertical position, operation to 12,000 rpm was started, and all cartridge heaters at the thrust end of the machine were energized. In order to increase the axial

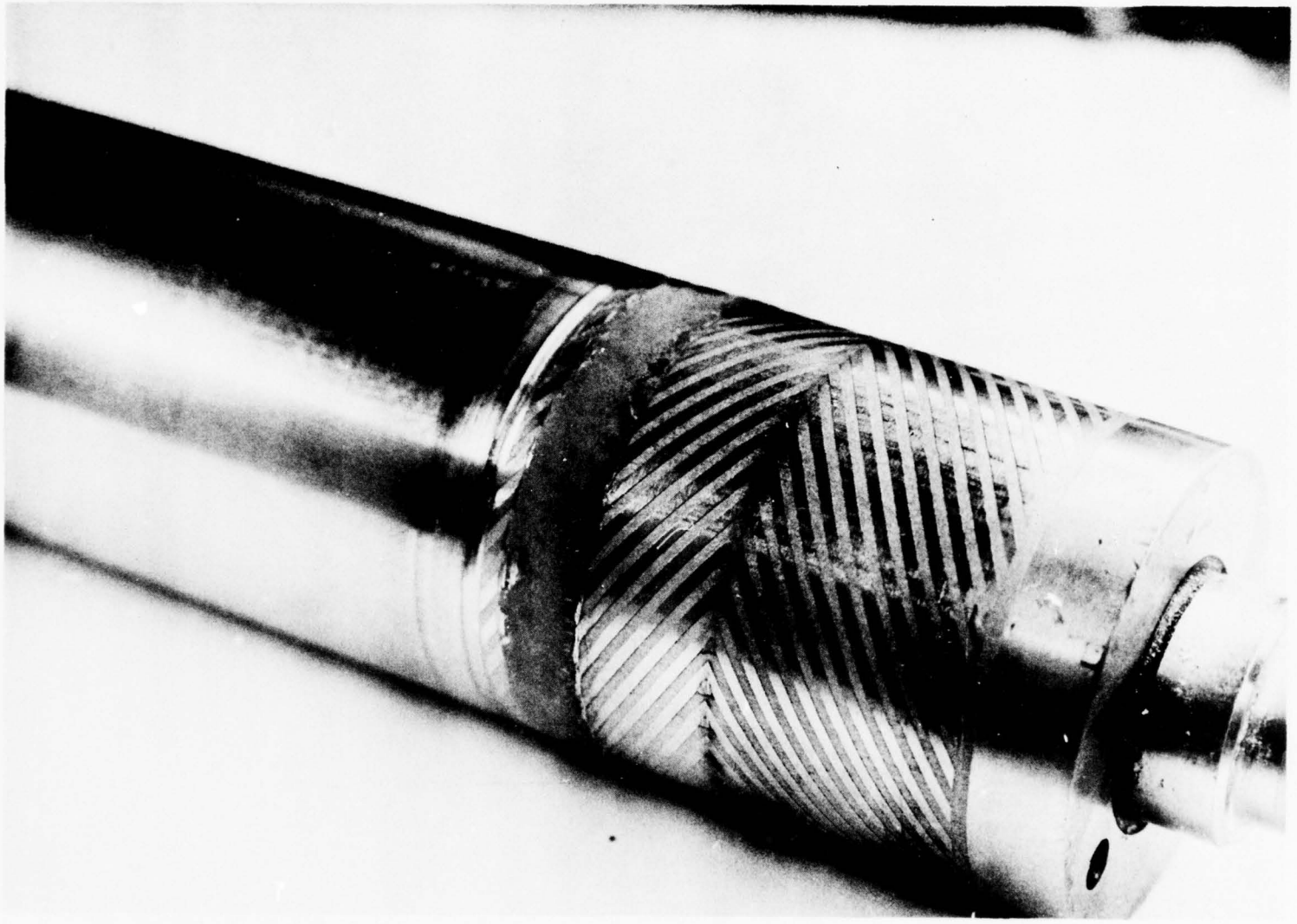

Fig. 10 Herringbone Journal Bearing Failure Due to Foreign Material Entering Bearing

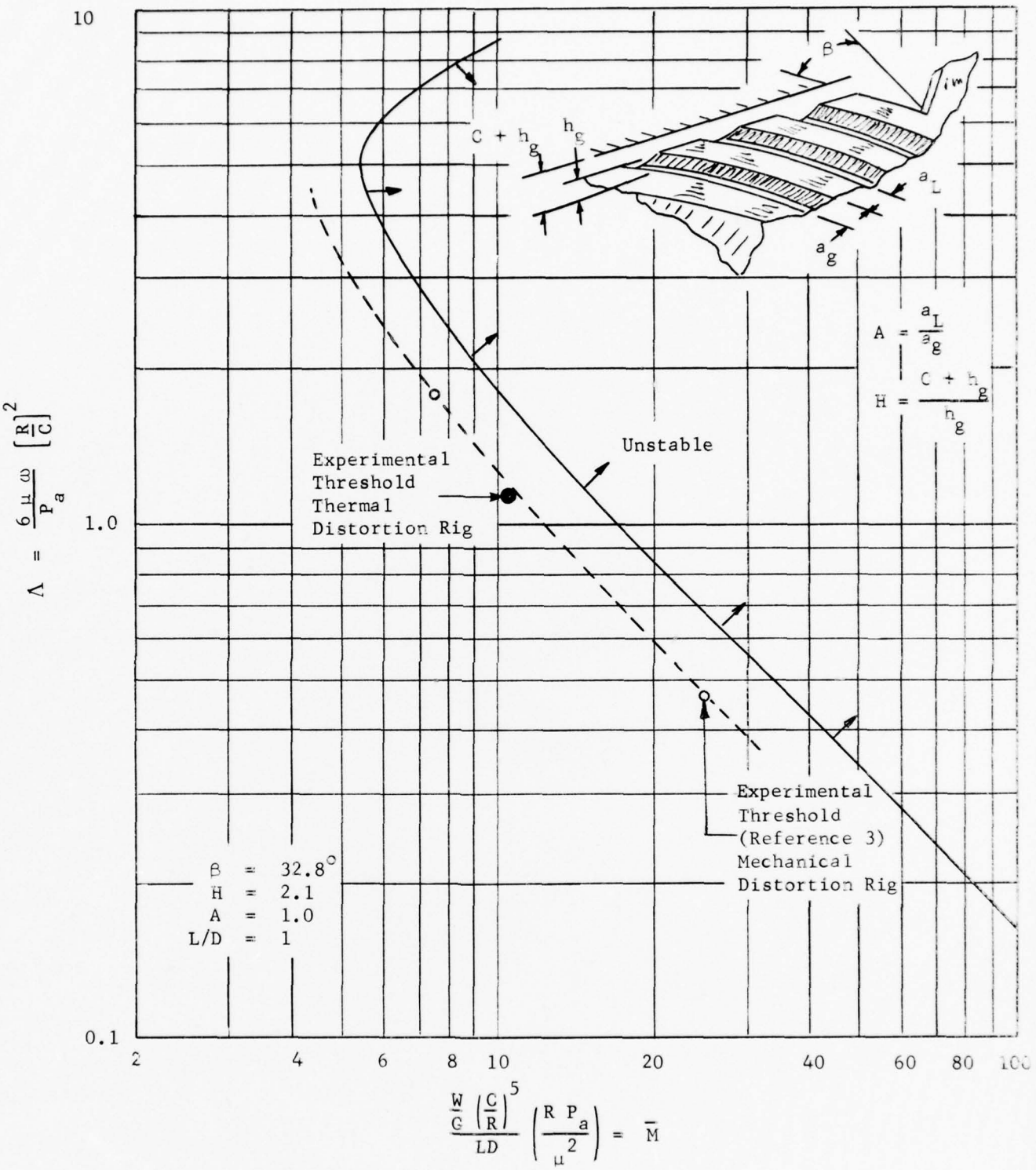

Fig. 11 Stability Map - Herringbone Journal Fully Grooved

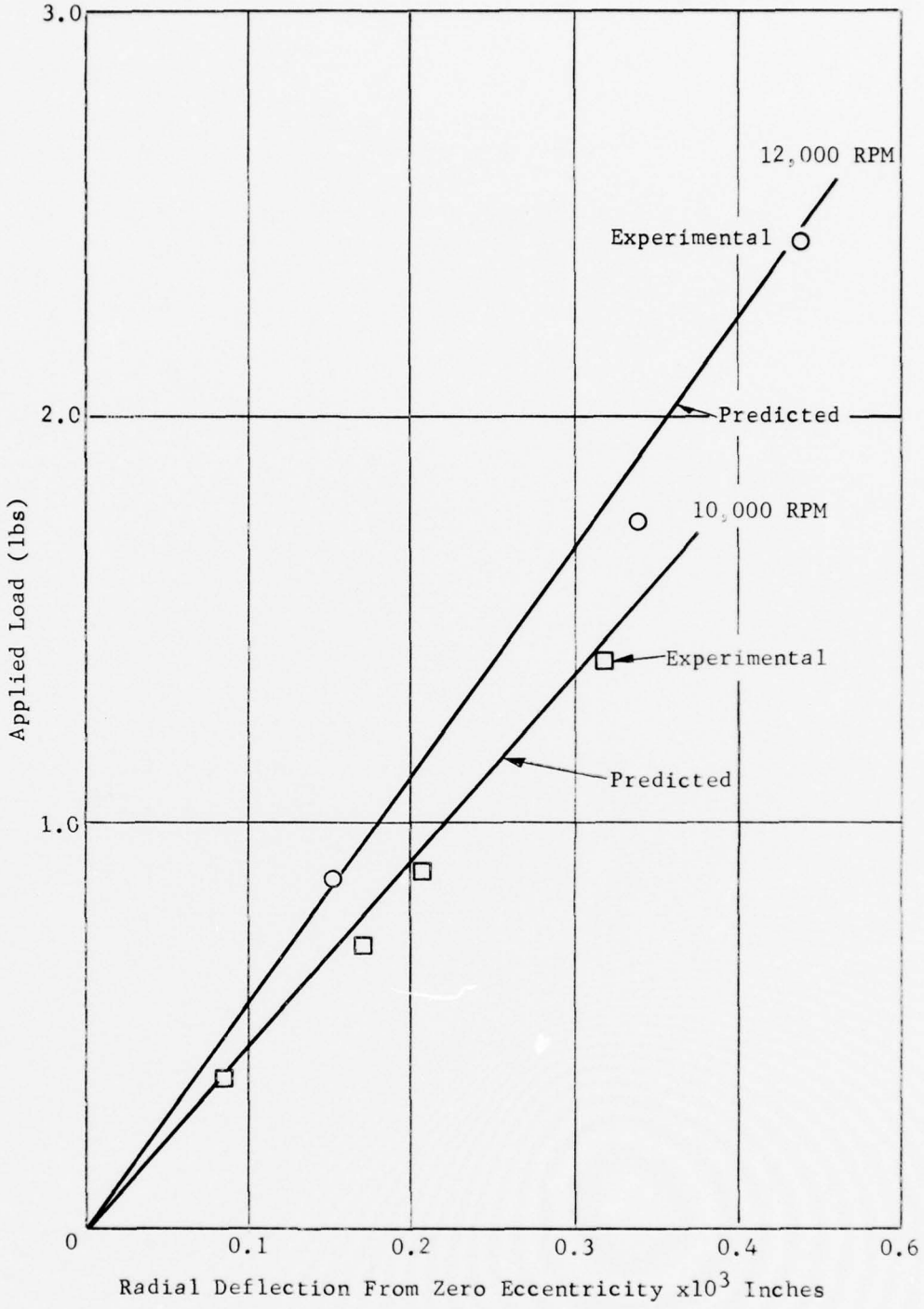

Fig. 12 Isothermal - Full Herringbone Journal Bearing Performance (C = 0.00086 inch) Thrust End Bearing

gradients, the thrust end was water-cooled using cooling coils. The rig operating in the shaft vertical condition is illustrated in Figure 13 during the gradient test.

During the heating cycle, the rig became unstable, necessitating reducing the operating speed. As a result, the threshold speed was monitored along with bearing temperatures during the heating cycle. The results of both the threshold speed change and the bearing temperature variations are plotted on Figure 14. After 30 minutes, the threshold speed began to increase and continued to increase throughout the heating cycle. During this heating cycle, the load capacity as well as the threshold speed of the bearing were checked. As noted from Figure 14, the average bearing temperature reached approximately 500°F. This temperature represents an increase in gas viscosity over room temperature from 2.7×10^{-9} to 4.1×10^{-9} lb-sec/in^2. The increase in viscosity would reflect an increase in both threshold speed and load capacity. However, Figure 14 illustrates a decrease in threshold speed. This is attributed to an increase in bearing radial clearance. Using the experimental threshold map of Figure 11, and the threshold speed of Figure 14, the effective bearing clearance was computed and plotted on Figure 15. The effective clearance curve reflects that clearance required to produce the stability speeds of Figure 14 including the effect of viscosity change. In addition, the average temperature difference between journal and bearing was calculated from the change in clearance and plotted on Figure 15. In summary, therefore, the threshold speed was used to determine effective bearing clearance. This clearance was used to predict load capacity of the thermally distorted bearing. The predicted results were compared to experimental for verification of the ability to analytically predict performance of a thermally distorted bearing.

After 120 minutes of heating, the number of heaters energized were modified to include four thrust and four bearing heaters. After approximately 160 minutes, all heaters were turned off. During the changes in energized heaters, the threshold speed was checked and the effective clearance determined. Load capacity was also determined at 145 and 215 minutes. Figure 16 outlines the bearing temperature during the complete test. Included on this figure is a tabulation of computed versus actual load displacement characteristics of the bearing. The computed characteristics as previously indicated are based upon the effective clearance in the bearing as determined from the stability characteristics. As noted, the actual displacements under load are within 50 microinches of predicted and in most cases are within 20 microinches. The trends in load capacity follow the predicted very closely. These results indicated that the bearing performance in terms of both stability and load characteristics can be determined very accurately if the effective clearance resulting after thermal distortions can be determined. As noted from Figure 17, which depicts the clearance with and without thermal gradients, the bearing indicates considerable out-of-roundness as a result of the gradients. In addition, from the observed bearing temperatures on Figure 16, there is also a bell-mouth plus taper condition existing in the bearing. Despite these distortions, the bearing tended to average out the variations and function with an average clearance. These results follow the same trend observed when mechanical distortions were induced into the bearing.

The type of overall gradients induced in the test rig during the heating and cooling cycles can be noted from Figures 18 through 21. These figures represent rig temperature at time 85, 110, 145, and 215 minutes, respectively. Considering the bearing region only, axial gradients to 120°F per inch, radial gradients to 160°F per inch, and circumferential gradients to 133°F per π radians were

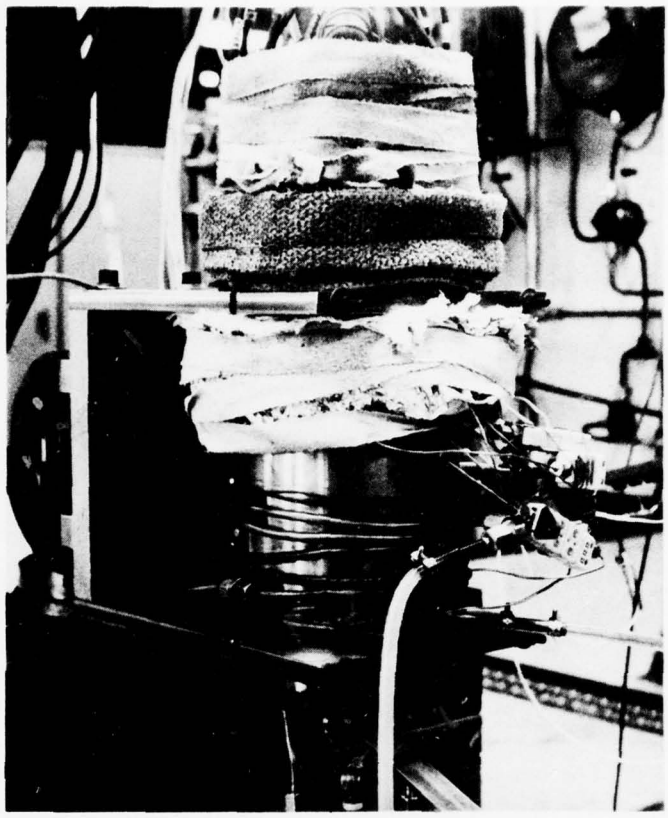

Fig. 13 Thermal Gradient Rig During Gradient Test

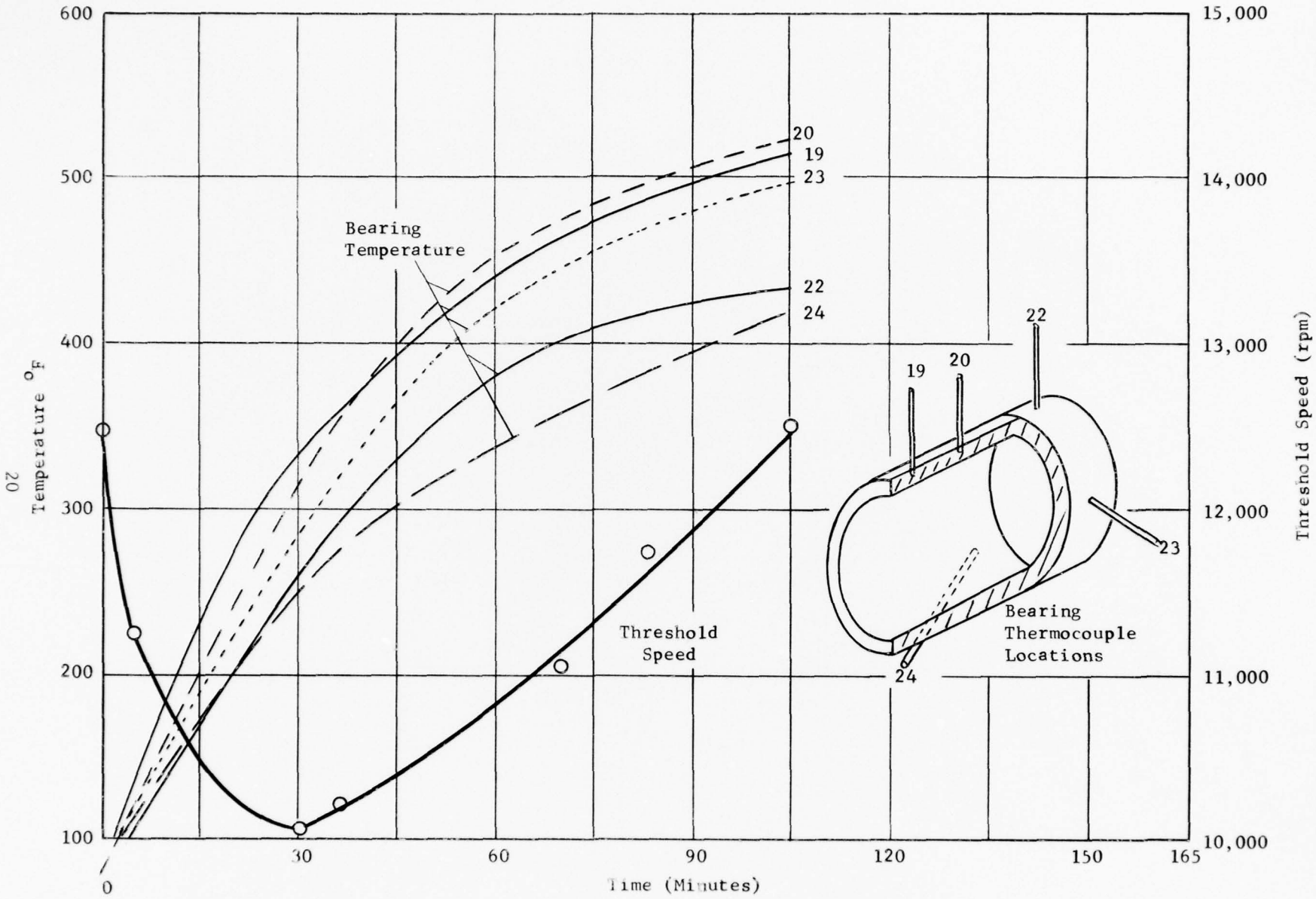

Fig. 14 Effect of Temperature Gradients on Stability of Herringbone Journal Bearing

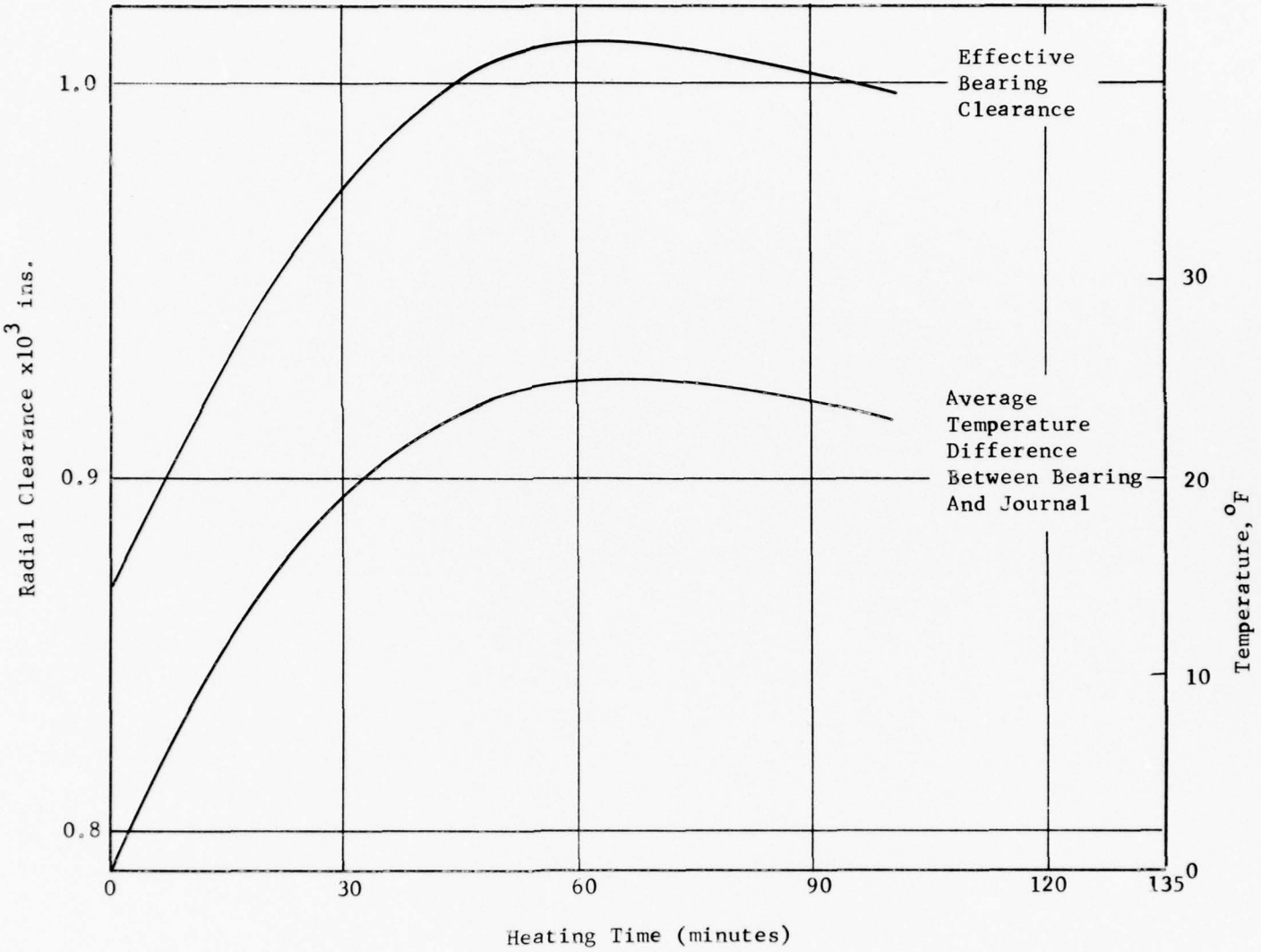

Fig. 15 Effect of Heating Cycle on Bearing Clearance

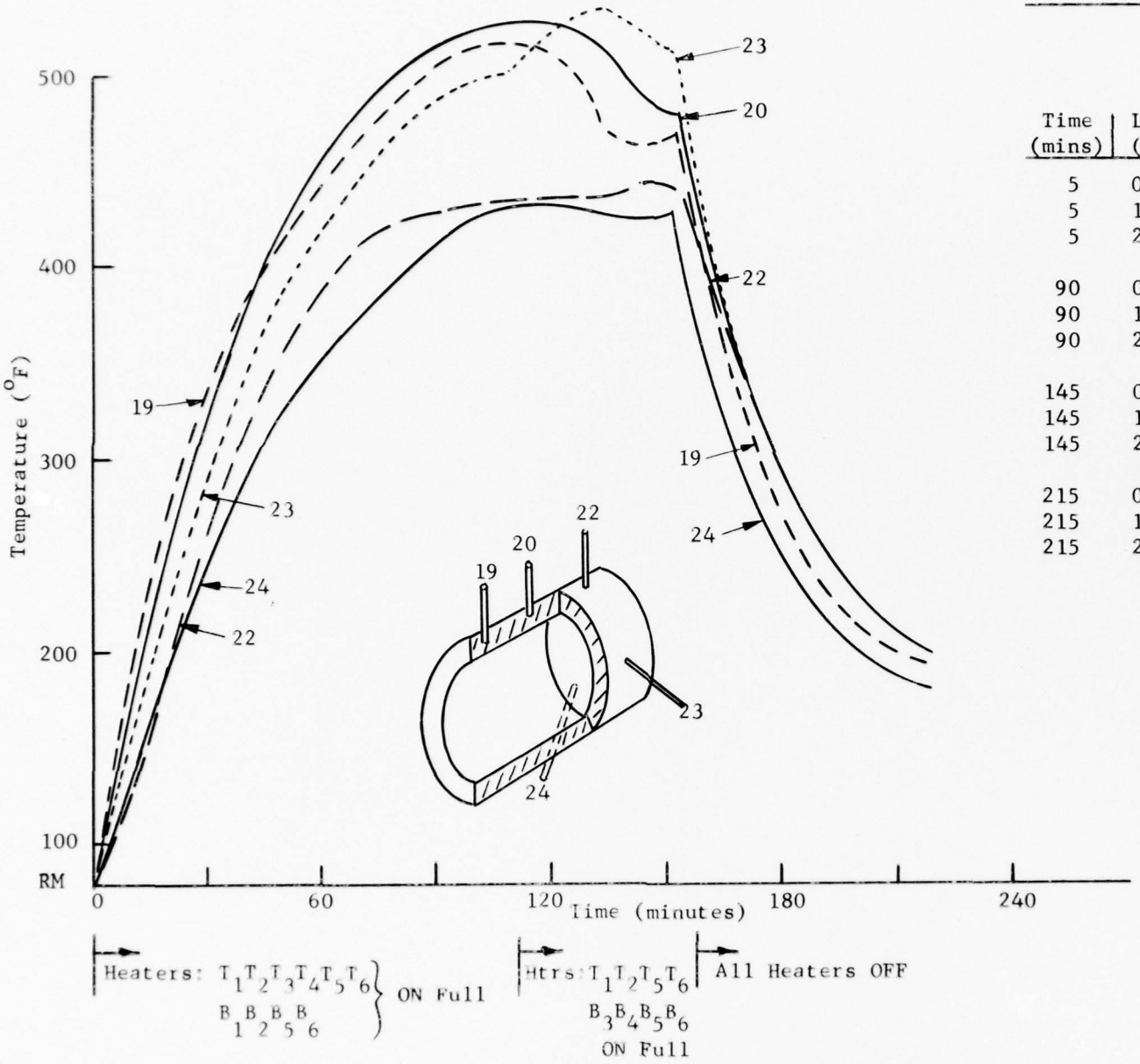

LOAD CHARACTERISTICS DURING TEST

Time (mins)	Load (lbs)	Radial Displ of Shaft Center From Bearing Center x10^3 ins.	
		Computed	Actual
5	0.87	0.152	0.177
5	1.74	0.304	0.316
5	2.44	0.426	0.422
90	0.87	0.148	0.150
90	1.74	0.297	0.272
90	2.44	0.415	0.382
145	0.87	0.127	0.127
145	1.74	0.254	0.208
145	2.44	0.339	0.318
215	0.87	0.122	0.132
215	1.74	0.244	0.262
215	2.44	0.341	0.370

Fig. 16 Effect of Temperature Gradients on Load Capacity of Herringbone Journal Bearing

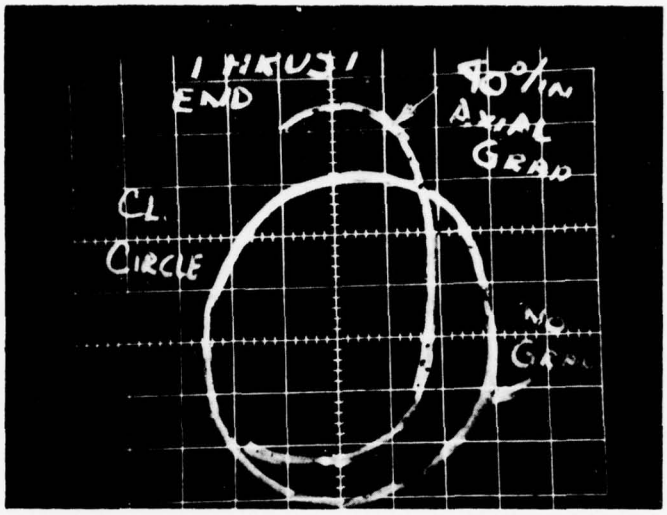

Fig. 17 Effect of Axial Gradients on Diametral Clearance

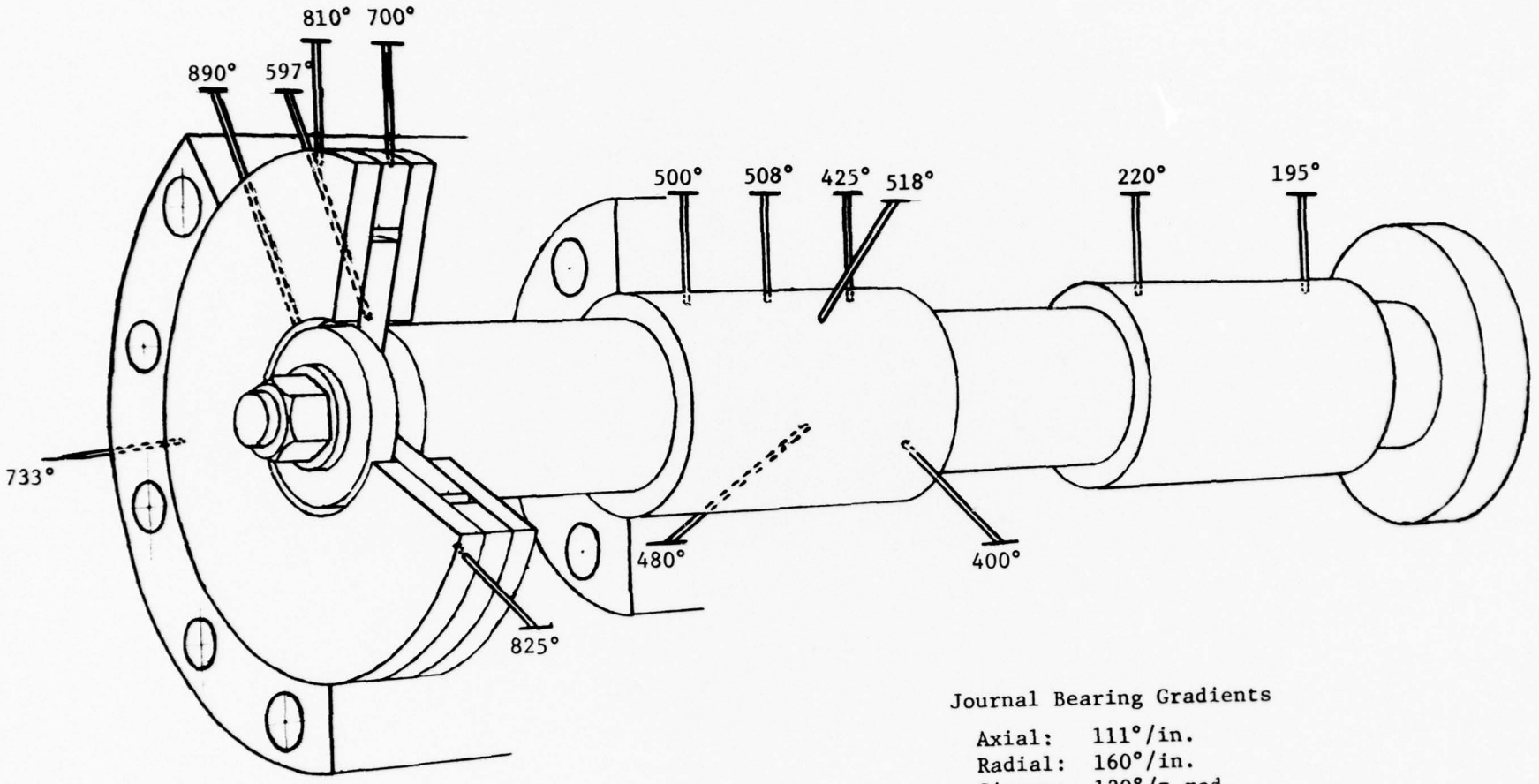

Fig. 18 Temperature Distribution After 85 Minutes
(Herringbone Bearing Test)

MTI-5870

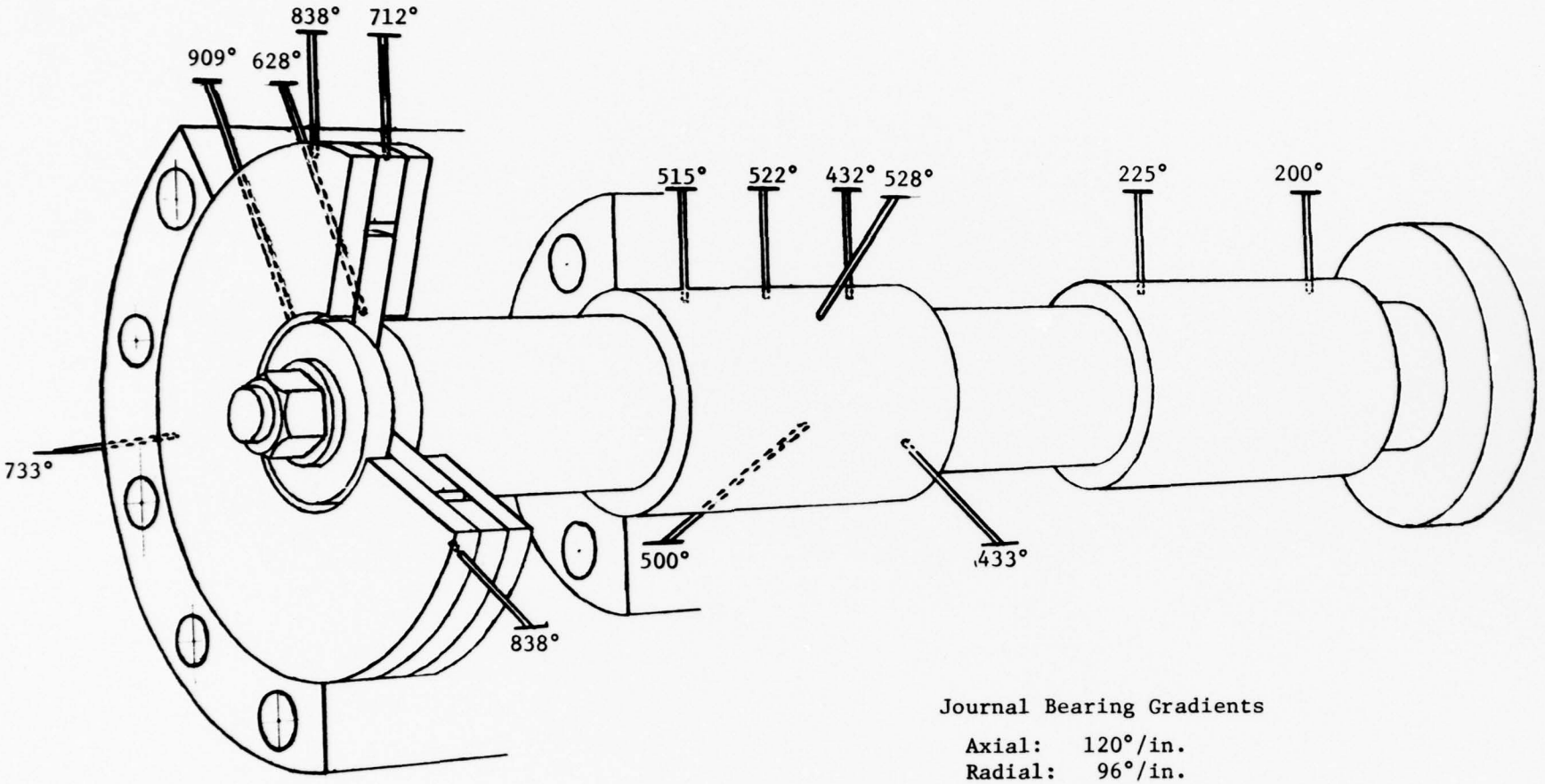

Journal Bearing Gradients

Axial: 120°/in.
Radial: 96°/in.
Circum: 102°/π rad.

Temperature Distribution at 110 mins.

Fig. 19 Temperature Distribution At 110 Minutes
(Herringbone Bearing Test)

MTI-5871

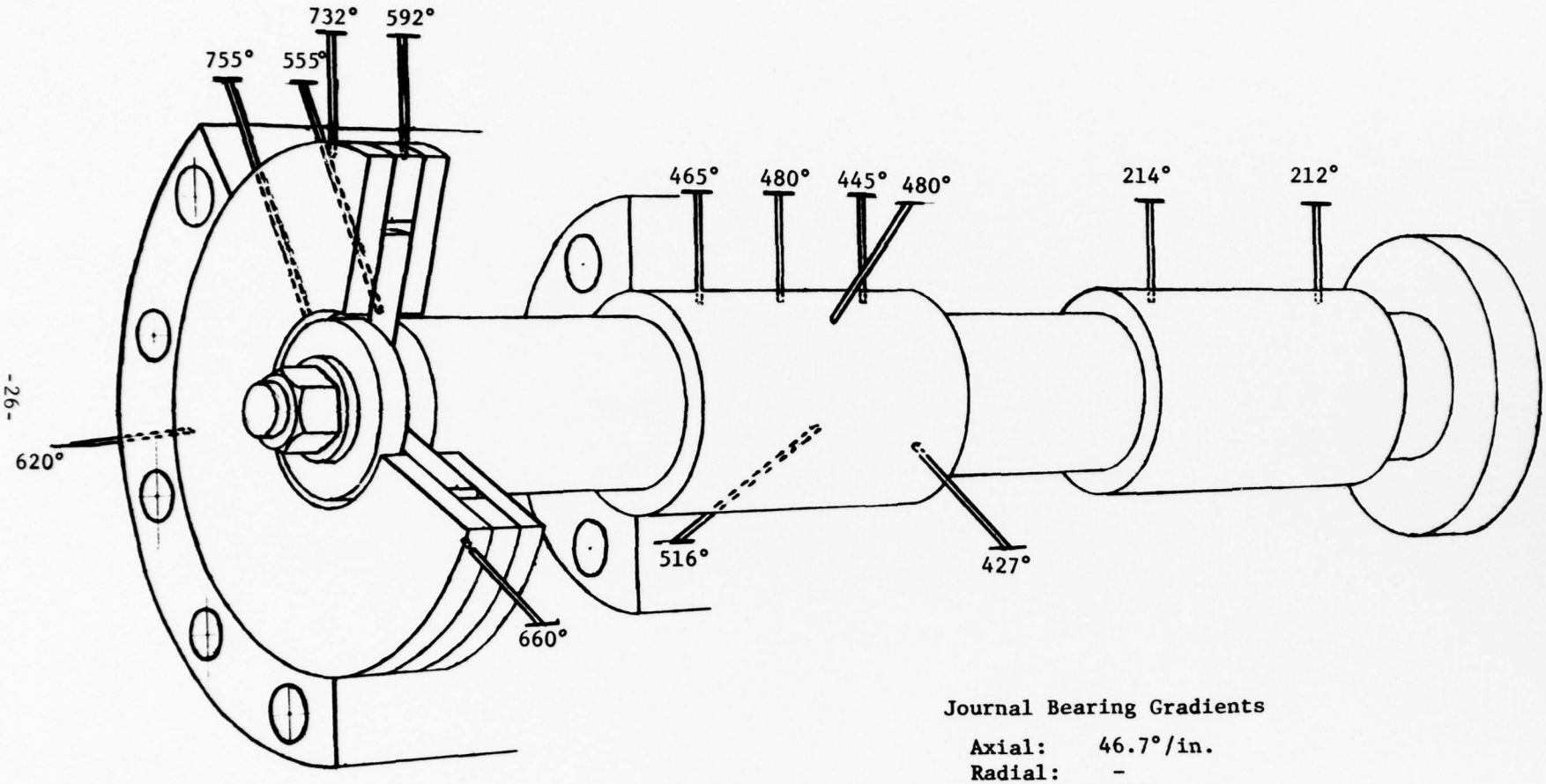

Fig. 20 Temperature Distribution At 145 Minutes
(Herringbone Bearing Test)

MTI-5869

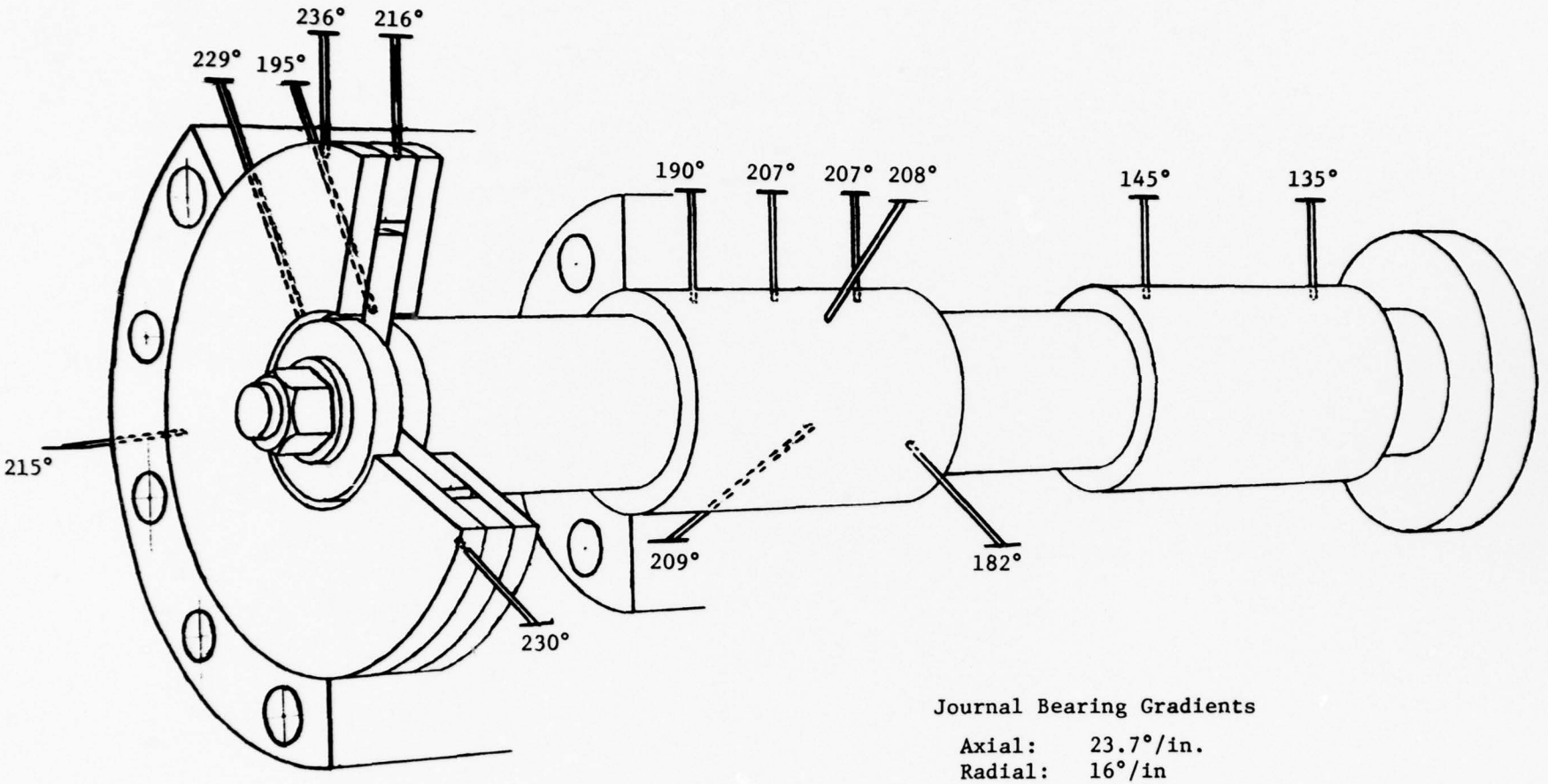

Fig. 21 Temperature Distribution At 215 Minutes
(Herringbone Bearing Test)

MTI-5868

experienced. These gradients were considered in excess of the normal gradients to be expected in turbomachines. However, despite this, the bearing continued to operate satisfactorily with predicted performance. It should be pointed out that due to the distortion, minimum running films in the bearing were reduced. This indicates that operation of this bearing would be limited to eccentricity ratios less than 0.5 under the gradients imposed.

It is interesting to note that gradients in the thrust bearing region were also very high. For these evaluations, a hydrostatic thrust bearing was utilized. At the extreme temperatures of Figure 9, the thrust plates warped sufficiently to cause leakage of the pressure behind the thrust plate and limited maximum thrust loads. Upon completion of the tests, permanent distortion of the thrust plates was noted. Maximum temperatures imposed on the thrust plates during the tests reached 1050°F. As noted during the tests with the Hastelloy X material, there is a tendency for dimensional instability at temperatures above 1000°F. In addition, the material stability tests were conducted without prestressing the components. In the actual rig operation, the thrust plates were held in compression. It was felt that this might add to the dimensional stability problem. The degree of distortion encountered was less than 50 microinches across approximately four inches. This, however, was sufficient to cause leakage around the static seal formed by the thrust plate and the housing. It was further felt that this type distortion would be typical for high temperature operation and would necessitate consideration in the initial design phase to accommodate it. No permanent distortion was evidenced in the journal bearing region of the rig or of the thrust runner. These areas, however, did not reach the 1000°F temperature range of the thrust stators.

Hydrodynamic Thrust Bearing Evaluations

As previously indicated, during the hydrodynamic thrust bearing evaluations, hydrostatic journal bearings were used for radial support. The purpose of the evaluations conducted was basically directed toward verifying the ability to predict hydrodynamic thrust bearing performance when subjected to thermal distortion. This presupposes that the exact type and degree of distortion can be found. Unfortunately, this is an extremely difficult task and is complicated by the fact that temperatures in the thrust bearing region reach 900°F. Therefore, an indirect method of predicting performance was used where it was necessary to assume the type of distortion. There was, however, physical experimental evidence to verify the assumptions used. The procedure can be outlined briefly as follows:

As seen from Figure 22, the total thrust bearing clearance should be the difference between the spacer thickness and the thrust runner thickness. When the rig is assembled at room temperature, the measured end play of the shaft was found to be less than the difference between spacer and runner thickness. This difference is due in part to squareness variation and partly due to distortion of the thrust plate faces under the assembled clamping action. The measured end play was corrected for the measured unsquare conditions and the difference between this figure and theoretical play that should exist, was attributed to distortion.

The rig was then heated in a static condition and the end play was measured during the heating and cooling cycles. The temperature of both runner and spacer was measured to determine any change in end play due to differential temperatures.

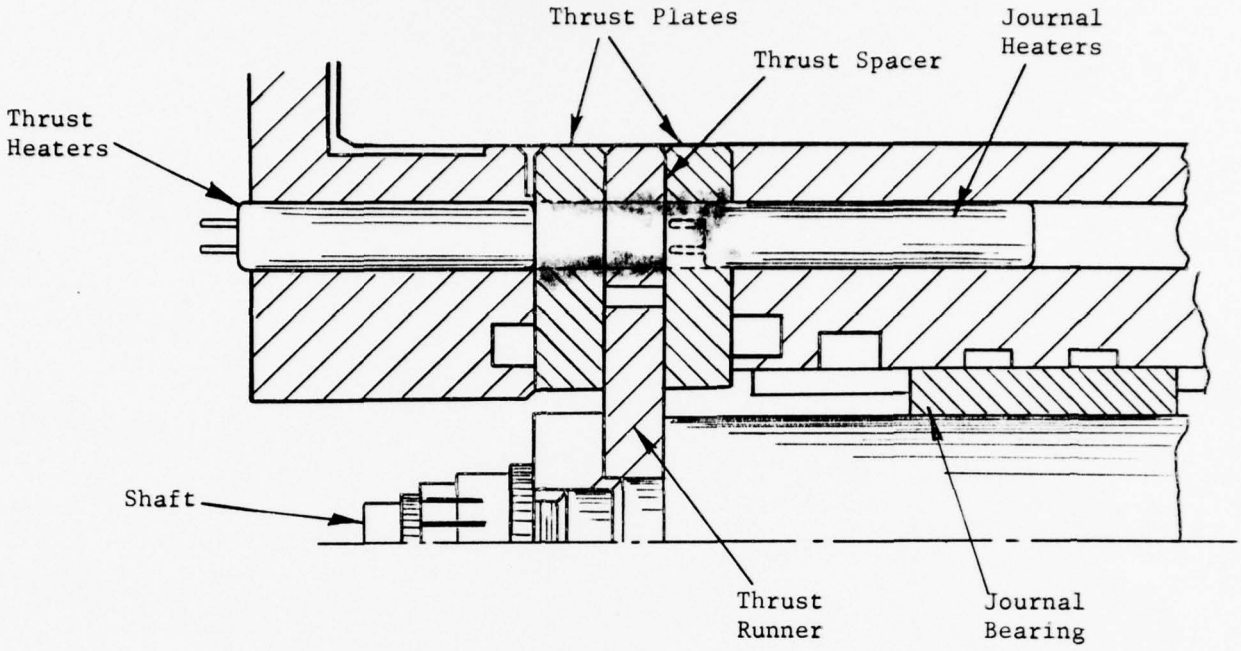

A. Thrust Bearing Assembly

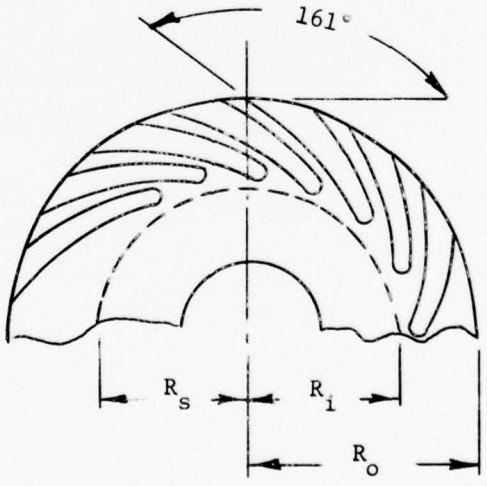

R_o = 1.312

R_i = 0.87

R_s = 0.944

No. of Grooves: 12
Groove Depth: .00157
$\frac{\text{Groove Width}}{\text{Ridge Width}}$ = 1.58

B. Hydrodynamic Thrust Runner Design

Fig. 22 Thrust Bearing Configuration

Beyond this, changes in end play were attributed to distortion of the thrust plates.

The distortions during both initial assembly and during the thermal cycle tend to reduce the effective bearing clearance. Depending upon whether the distortion is dishing or crowning of the thrust plates, the reduction in effective clearance can vary between 40 and 60 percent of the total distortion. Contact marks between runner and thrust plate during actual running, infer that crowning of the thrust plates occurred. Therefore, 60 percent of the loss in clearance attributed to distortion was applied to determine the effective bearing clearance.

Performance of the bearing over the heating cycle was determined analytically using the effective bearing clearance. The rig was then operated over the same heating and cooling cycles with the load deflection characteristics determined at varying intervals during the test. The effective clearance necessary to produce these characteristics was determined analytically. In order to determine how well actual performance followed predicted, a comparison was made between effective measured bearing clearance statically and the effective bearing clearance necessary to produce the dynamic characteristics. The difference indicates how closely performance can be predicted under thermally distorted conditions. With this brief description of the experimental procedure, the details of the results may be more clearly understood.

The thrust bearing was assembled with a built-in axial clearance (total) of 0.00357 inches. End play measurements indicated a clearance of 0.00316 inches. The additional loss in end play of 0.00041 was attributed to distortion resulting from the compressive clamping stress on the thrust plates. Operation indicated this distortion was primarily coning of the thrust plate which would tend to reduce the effective bearing clearance by 60 percent of the crown height. The resulting effective bearing clearance prior to heating the bearing therefore was 0.00332 inches.

Additional end play checks of the bearing were made during a static heating cycle. Variations in end play were attributed primarily to additional crowning of the thrust plates. Figure 23 outlines the measured temperatures in the thrust bearing region, and the change in measured end play of the thrust system.

During the initial heating cycle, a slight increase in end play was observed indicating the initial transient temperature condition tended to reduce the distortion condition. After 30 minutes, the end play began to decrease until the heaters were cut off. The differential temperature between runner and spacer represented a loss of approximately 0.00015 inches in end play during the heating cycle. When the heat was removed, the differential temperature between runner and spacer dropped from 50°F to 10°F in three minutes. This tended to open the clearance 0.00012 inches. However, the transient condition induced additional distortion of the thrust plates with an overall sudden decrease in total play in a ten minute period. After the initial transient, the end play increased and after four hours returned to within 0.00006 inches of initial measurements.

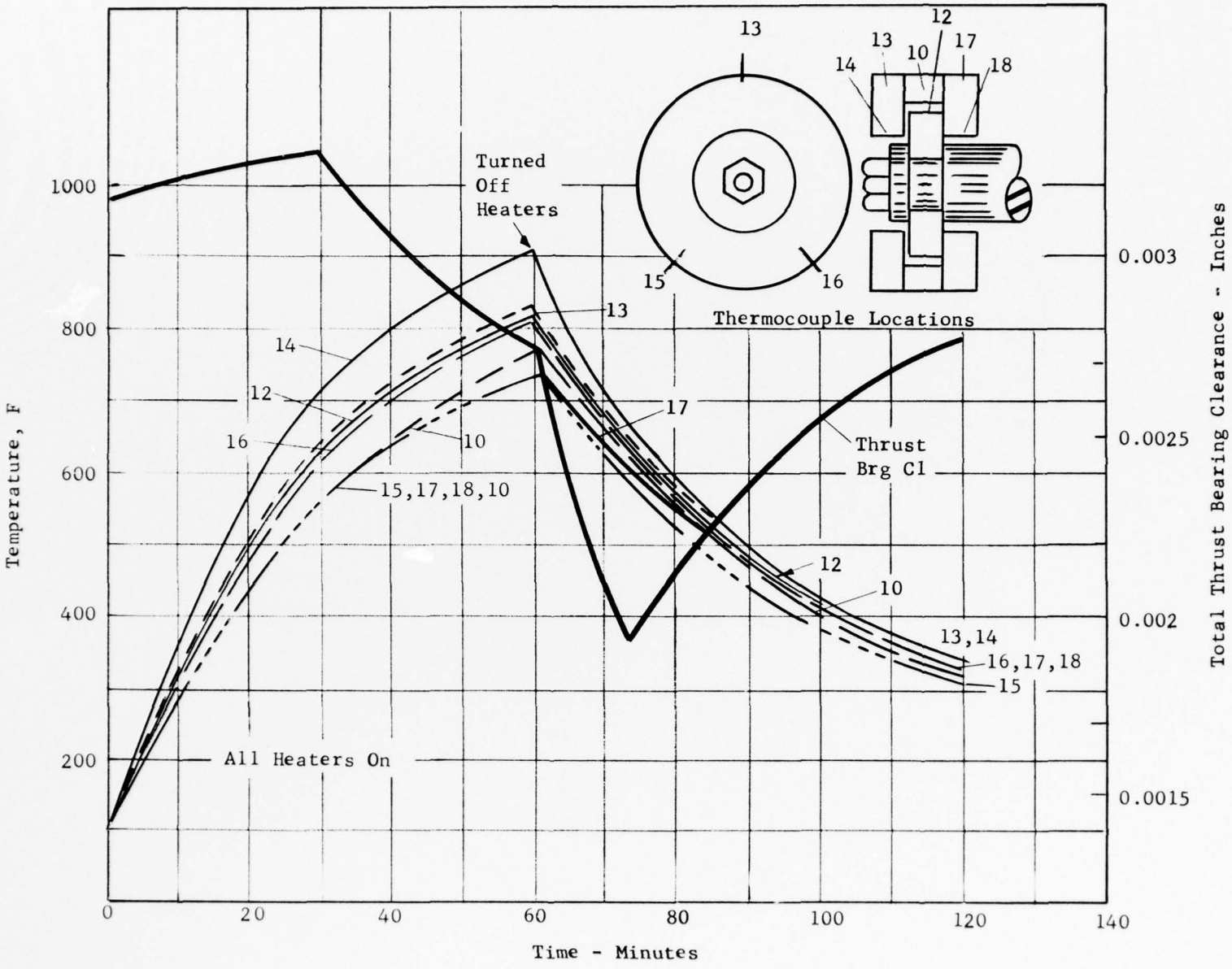

Fig. 23 Effect of Thermal Gradients on Spiral-Groove Thrust Bearing End Play

MTI-5333

As previously indicated, the end play measurements do not necessarily reflect the effective bearing clearance. This is the nominal clearance at which the bearing attempts to operate. When the thrust plates distort inward to remove end play, the effective clearance is reduced only a percentage of this clearance change depending upon the type of distortion. During actual operation of the thrust bearing under distorted conditions, contact occurred at the inboard edge of the inboard thrust plate and runner as shown on Figure 24. This inboard plate was the heavily loaded thrust member. On the light loaded plate, contact occurred both outboard and inboard. This implies that the inboard plate distorted in a crowned condition while the outboard tended to remain reasonably flat with some light dishing occurring. The interpretation of these contact areas is that crowning is the major cause of end play change. Therefore, following the mechanical distortion experimental results, the loss in effective clearance was taken as 60 percent of the distorted crown height as determined from the end play measurements. It should be pointed out that the contact marks were induced during test by loading the bearing to contact. Although not apparent from Figure 25, there was no measurable bearing damage discernible from the induced contact.

Following this approach, it is possible to tabulate end play and effective bearing clearance in Table I.

TABLE I

EFFECTIVE THRUST BEARING TOTAL AXIAL CLEARANCE

Time Mins.	End Play $\times 10^3$ ins.	Runner to Spacer Thermal Growth $\times 10^3$ ins.	Crown Distortion $\times 10^3$ ins.	Effective Axial Bearing Clearance $\times 10^3$ ins.
0	3.16	00	.41	3.32
30	3.31	-.18	.09	3.52
45	2.96	-.18	.43	3.31
60	2.76	-.15	.66	3.17
75	1.96	-.03	1.58	2.62
90	2.46	-.03	1.08	2.92
105	2.61	-.02	.94	3.01
120	2.76	-.02	.77	3.13

(-) Indicates loss in play.

The resulting effective axial clearance does not reflect the influence of frictional heating or cooling effect of windage around the rotating thrust runner. At the maximum operating speed of 20,000 rpm these influences should not seriously alter the temperature distribution. During the heating and cooling cycles while operating the unit over the speed range, the temperature distribution as shown on Figure 25 was recorded. As noted, the temperature changes indicate approximately the same slope and distribution although peak temperatures are approximately 70°F cooler. The assumption that the distortion of the thrust plates will follow the same trends as determined under static conditions, appears very reasonable. During the heating and cooling cycle, the load displacement characteristics of

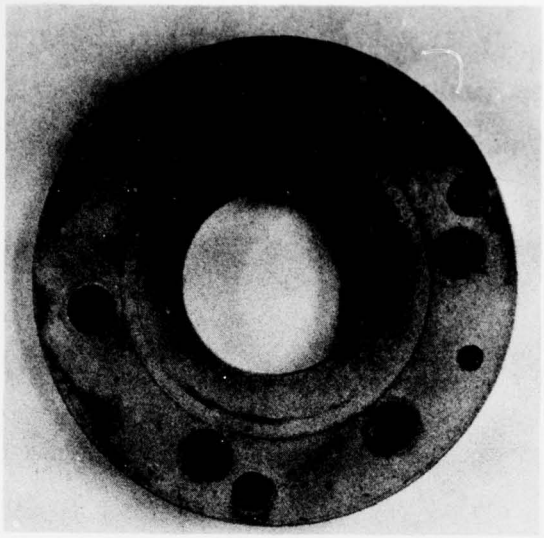

Outboard Thrust Plate

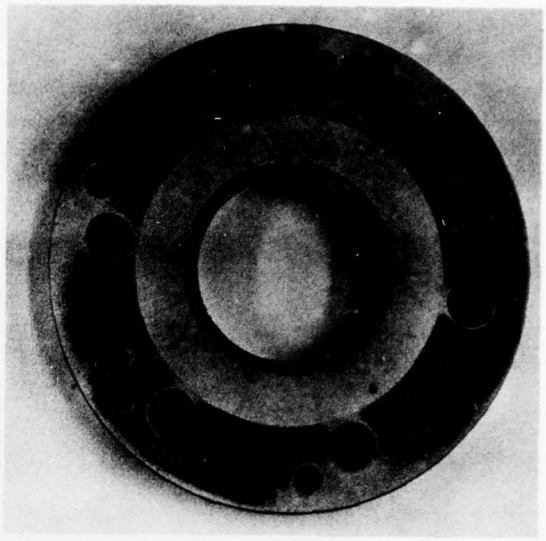

Inboard Thrust Plate

Outboard Face of Thrust Runner

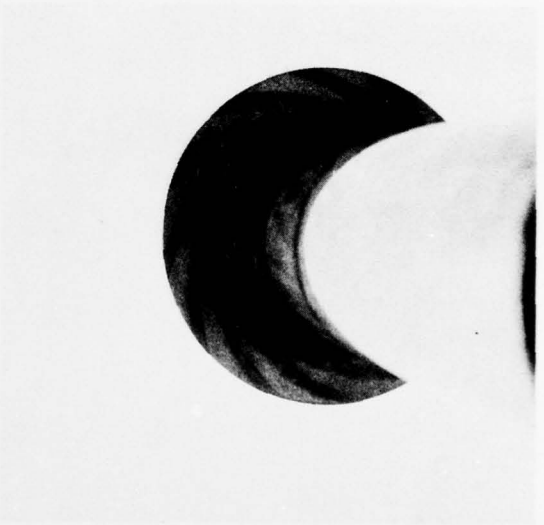

Inboard Face of Thrust Runner

Fig. 24 Hydrodynamic Thrust Bearing After Thermal Distortion Test

MTI-5877

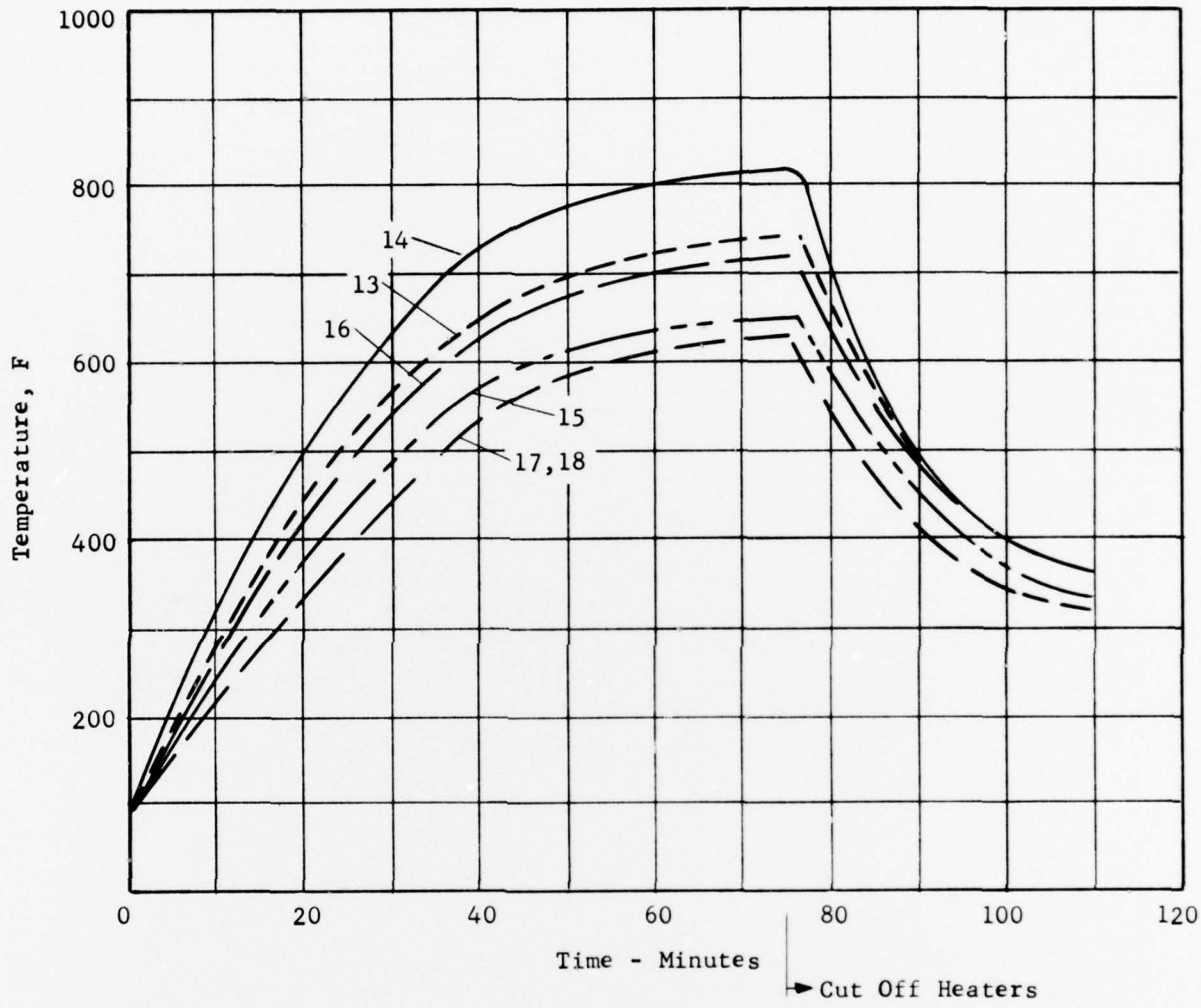

Fig. 25 Temperature, Spiral-Groove Thrust Bearing Test (Dynamic)

MTI-5833

the thrust bearing at 10,000, 15,000 and 20,000 rpm were determined. The tabulated measured results are outlined in Table II.

TABLE II

HYDRODYNAMIC THRUST BEARING
EXPERIMENTAL LOAD DEFLECTION CHARACTERISTICS

10,000 RPM			15,000 RPM			20,000 RPM		
Time (mins)	Load (lbs)	Displ. ($x10^3$ins)	Time (mins)	Load (lbs)	Displ. ($x10^3$ins)	Time (mins)	Load (lbs)	Displ. ($x10^3$ins)
0	-.48	0	0	-.48	0	0	-.48	0
(100°F)	.00	1.315		.00	1.988		.00	.792
	.48	1.755		.48	1.36		.48	1.052
	1.425	2.02		1.425	1.58		1.425	1.272
				2.75	1.712			
20	-.48	.00	27	-.48	.00		2.75	1.45
(400°F)	.00	1.25	(470°F)	.00	.965		3.75	Touch
	.48	1.93		.48	1.449	35	-.48	.00
	1.425	2.13		1.425	1.69	(550°F)	.00	.659
	2.67	Touch		2.75	1.84		.48	.965
70	-.48	.00	65	-.48	.00		1.425	1.23
(680°F)	.00	.57	(675°F)	.00	.439		2.75	1.34
	.48	.90		.48	.725		3.68	Touch
	1.425	1.183		1.425	.965	60	-.48	.00
78	-.48	.00		2.33	1.12	(670°F)	.00	.351
(630°F)	.00	.351	80	-.48	.00		.48	.572
	.48	.615	(600°F)	.00	.263		1.425	.835
	1.33	Touch		.48	.395		2.75	1.01
101	-.48	.00		1.425	.614		2.8	Touch
(370°F)	.00	.763						
	.48	1.14	98	-.48	.00	83	-.48	.00
	1.425	1.39	(375°F)	.00	.439	(550°F)	.00	.198
300	-.48	.00		.48	.79		.48	.351
(100°F)	.00	1.27		1.425	1.01		1.425	.572
	.48	1.71	300	-.48	.00	95	-.48	.00
	1.425	1.93	(100°F)	.00	1.095	(400°F)	.00	.316
	2.50	Touch		.48	1.492		.48	.572
				1.425	1.712		1.425	.747
						300	-.48	.00
						(100°F)	.00	.857
							.48	1.14
							1.425	1.36
							2.75	1.49

In order to provide a comparison between the experimental results and predicted results, the approach followed was to determine the axial thrust bearing clearance required to produce the experimental results. This, in turn, was compared to the effective clearance as previously determined.

The computed load deflection characteristics of the bearing configuration with 0.004 inch total clearance at 15,000 rpm are plotted on Figure 26 for 100°F, 460°F and 860°F. Similar plots were constructed for 10,000 and 20,000 rpm. Referring to Figure 26, the left-hand position of the curve reflects the load capacity on one thrust face while the right-hand side is the reverse thrust face. The right-hand portion of the curve actually reflects negative loads relative to the left-hand portion but was plotted as shown for convenience. At 0.002 inch end play, the load capacity is zero. For a load variation from −1 pound to +1 pound, the axial rotor displacement would vary from 0.00081 to 0.00319 or a displacement of 0.00238. As the total end play of the thrust bearing is reduced, the left-hand and right-hand portions of the curve move closer to each other by the reduction in end play. The intersections of the curves represent the midpoint or zero load point of the bearing. The final load capacity characteristic is the difference between the sum of the right and left side of the curves, remembering that the right-hand side has negative values of load.

The load deflection characteristics of the thrust bearing were calculated for axial total clearances of 0.004, 0.0035, 0.003 and 0.0023 inches. The data was plotted in the form of the experimental data, i.e: utilizing −0.5 pounds as zero axial deflection. The results are shown on Figures 27, 28 and 29 for 10,000, 15,000 and 20,000 rpm, respectively. Included on these plots are the experimental points of Table II. From this data it is possible to estimate the apparent bearing clearance necessary to produce the experimental results. This information is tabulated in Table III.

TABLE III

THEORETICAL BEARING CLEARANCE
TO PRODUCE EXPERIMENTAL RESULTS

10,000 RPM		15,000 RPM		20,000 RPM	
Time Mins.	Effective Axial Cl. x 10^3 ins.	Time Mins.	Effective Axial Cl. x10^3 ins.	Time Mins.	Effective Axial Cl. x10^3 ins.
0	3.5	0	3.4	0	3.3
20	3.8	27	3.4	35	3.5
70	3.2	65	3.0	60	3.0
78	2.8	80	2.6	83	2.6
101	3.1	98	2.9	95	3.0
300	3.5	300	3.5	300	3.3

A comparison can now be made between the effective bearing clearance that would be used to predict performance of Table I and the clearance necessary to produce the experimental results of Table III. This is shown on Figure 30. It is obvious that the effective bearing clearance of Table I could be used to predict performance and compared with final results. The actual procedure used essentially accomplishes the same thing and proved more convenient, having established the load deflection characteristics of Figure 27 through 29 prior to test. It also provides a clearer approach to reviewing the overall comparison. The time base of the data of Table I as plotted on Figure 30 was increased by 15

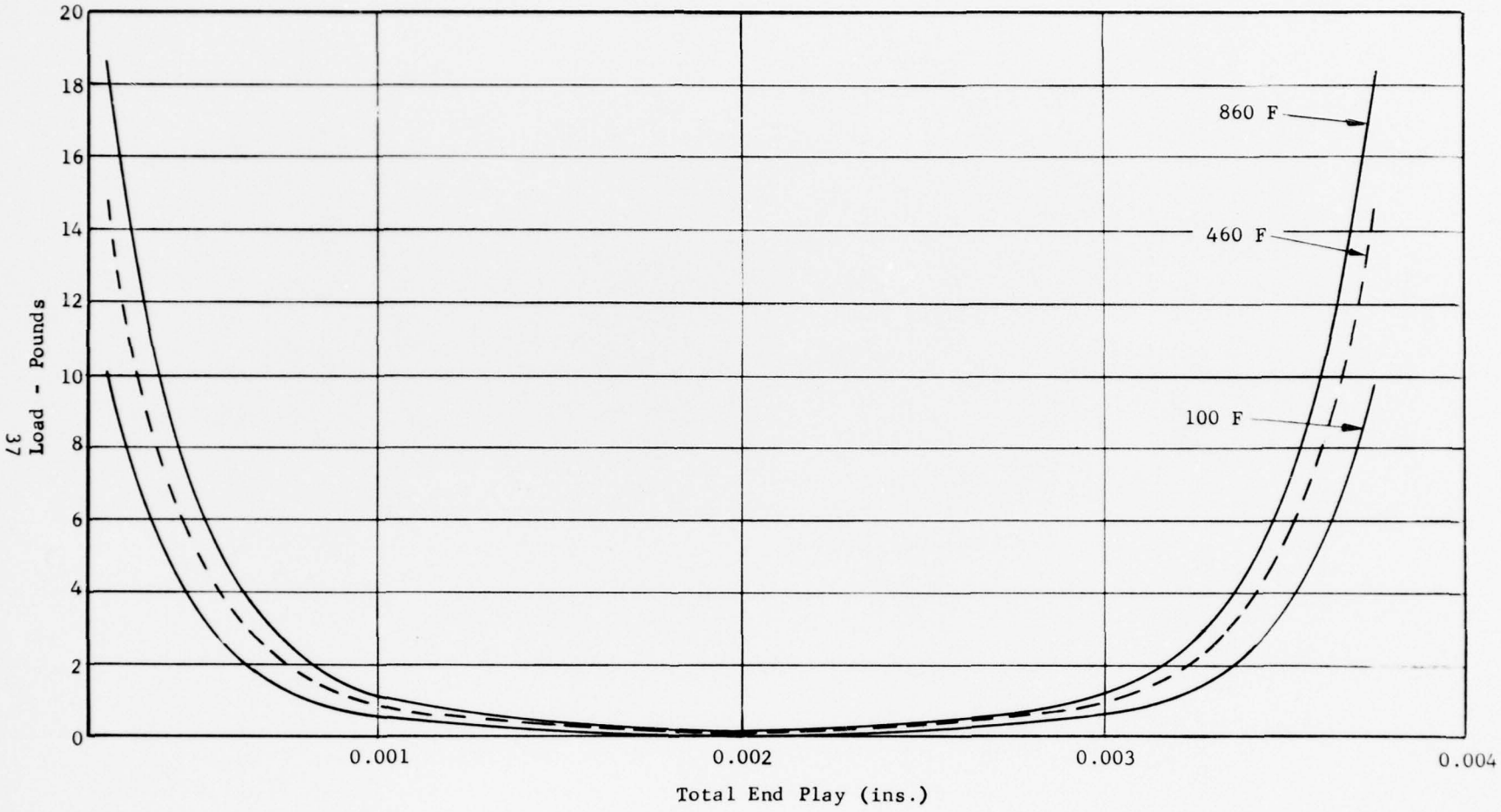

Fig. 26 Hydrodynamic Double-Acting Thrust Bearing Theoretical Performance At 15,000 RPM, 0.004 Inch End Play

MTI-5832

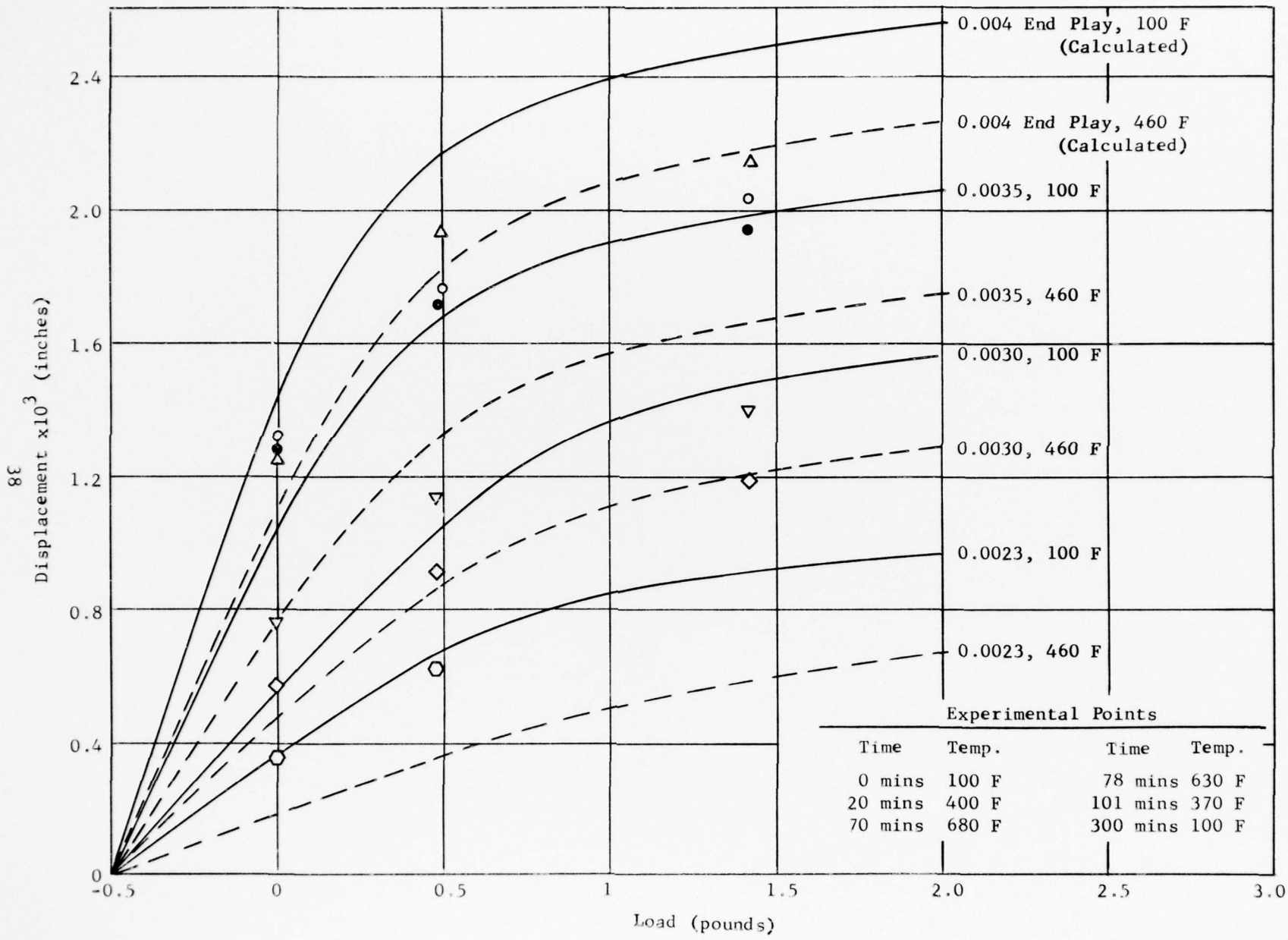

Fig. 27 Bearing Load Characteristics 10,000 RPM, Double-Acting Hydrodynamic Thrust Bearing

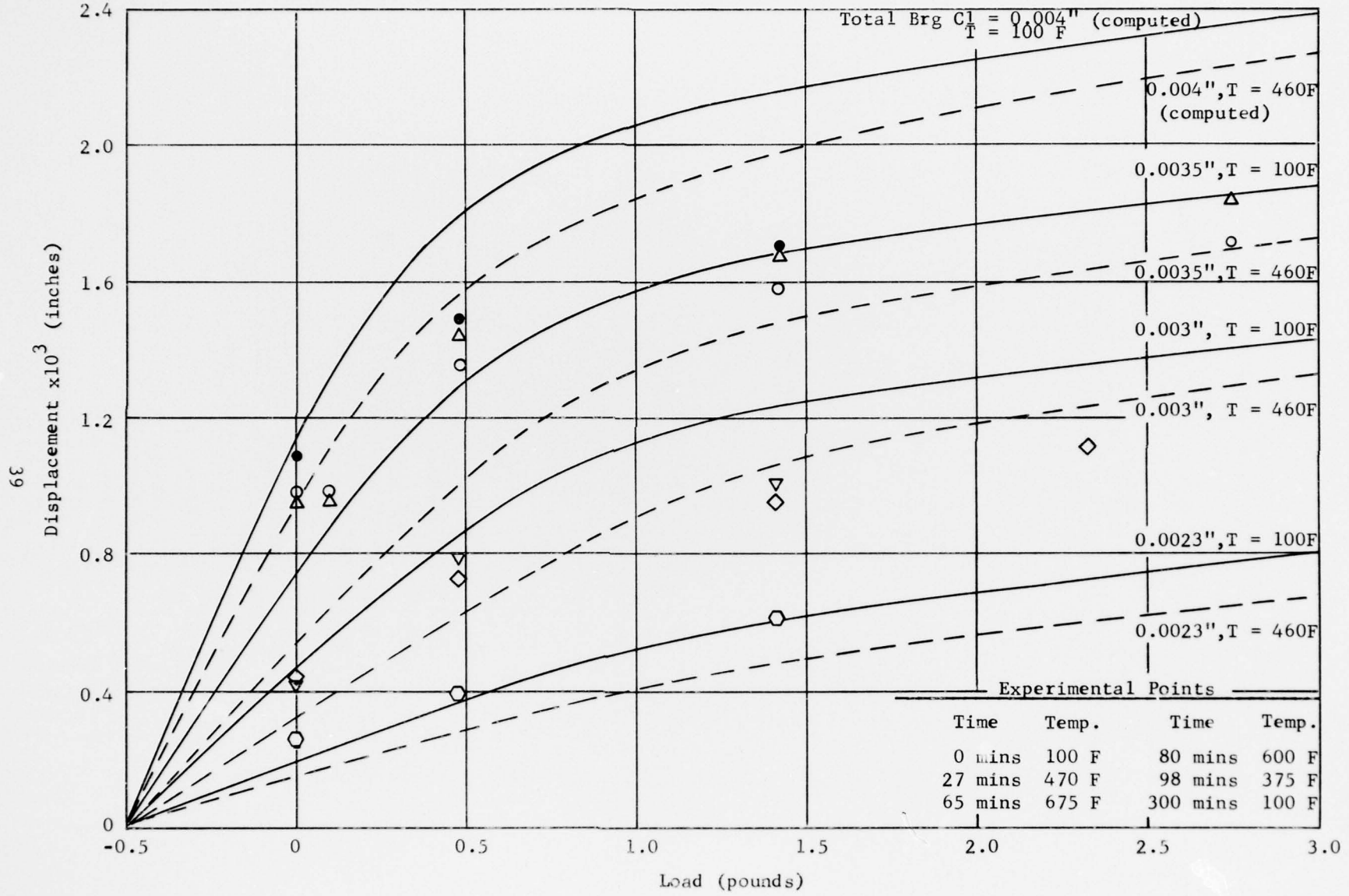

Fig. 28 Bearing Load Characteristics, 15,000 RPM
Double-Acting Hydrodynamic Thrust Bearing

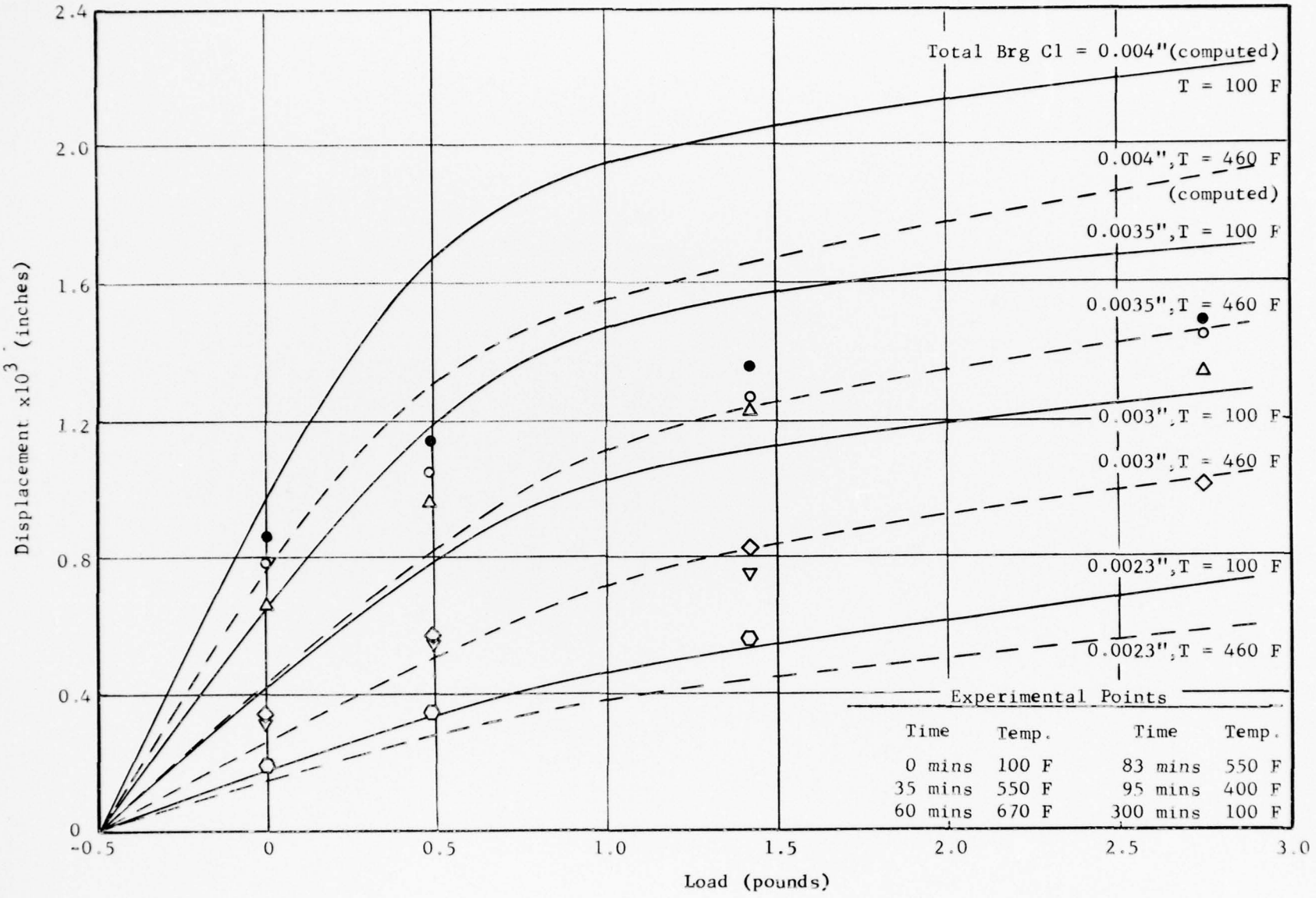

Fig. 29 Bearing Load Characteristics, 20,000 RPM
Double-Acting Hydrodynamic Thrust Bearing

minutes after the 60 minute data point because of the additional 15 minute heating time during dynamic tests. This places the heating cycle and cooling cycle of both static and dynamic tests on the same time base.

It may be noted from Figure 30 that the effective bearing clearance during operation tended to increase during the first 30 minutes of heating followed by a decrease during the remaining 45 minutes. This followed the statically measured trend during this period. As the heat was turned off, the operational clearance dropped and then increased, following the trend of the statically measured results. Experimental results followed predicted results within five percent, which is considered extremely good since the actual physical distortion of the bearing could not be measured directly.

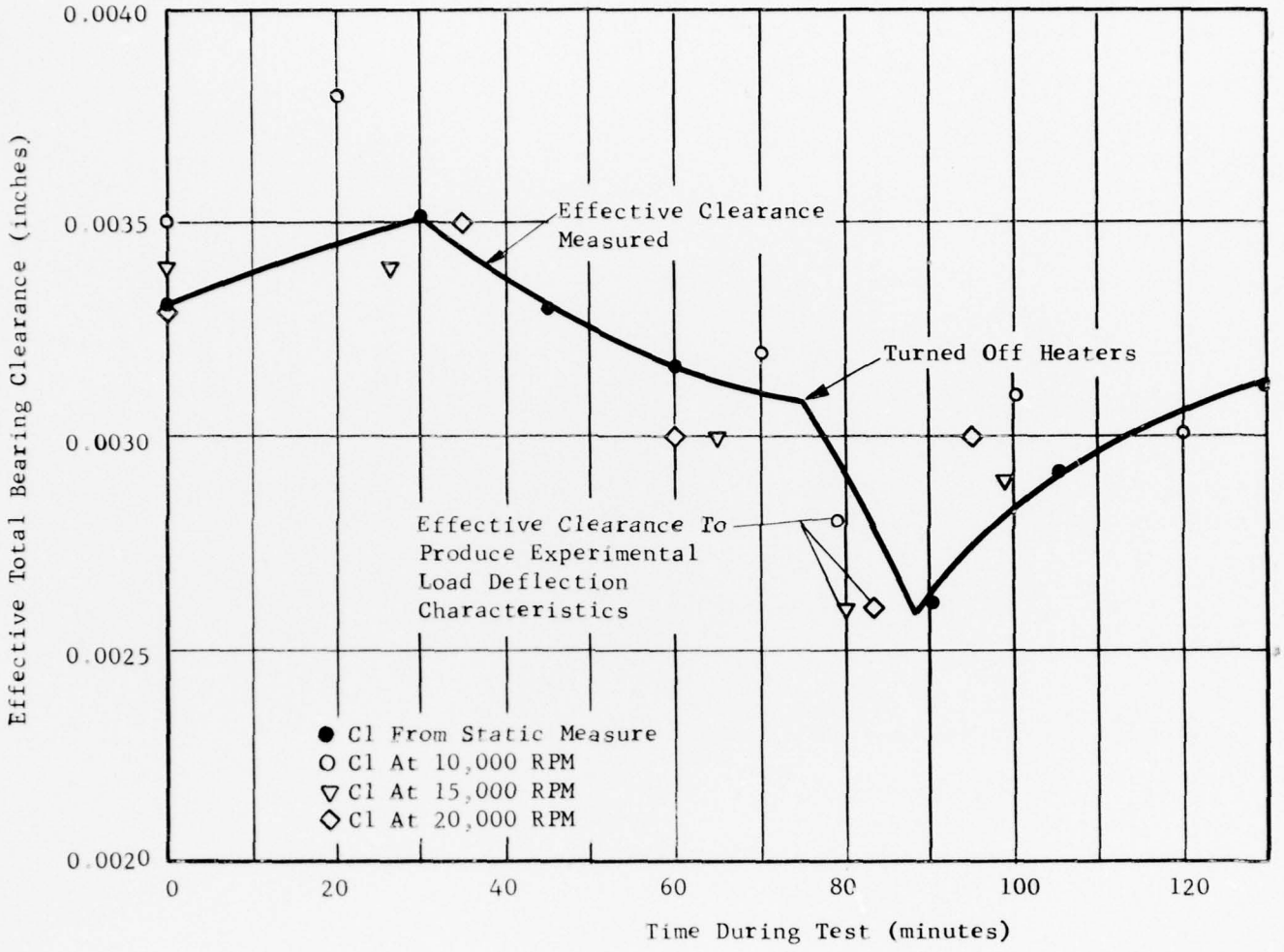

Fig. 30 Comparison Of Experimental And Predicted Test Results During Thermal Distortion (Hydrodynamic Thrust Bearing)

SECTION III

SUMMARY OF RESULTS OF NON-ISOTHERMAL OPERATION OF HYDRODYNAMIC BEARINGS

Herringbone journal and spiral-groove thrust bearings were subjected to operation under non-isothermal conditions. The distortions resulting from the induced thermal gradients could not be measured directly. However, through indirect means, it was established that bearing performance could be predicted by utilizing an effective bearing clearance. This effective bearing clearance was found to be the average bearing clearance while in a distorted condition. This same tendency was observed during mechanically induced distortion evaluations.

In the case of the herringbone journal bearing operation was conducted with axial bearing gradients to $120^{\circ}F$/inch, radial gradients to $160^{\circ}F$/inch and circumferential gradients to $133^{\circ}F/\pi$ radians. Under these conditions, the bearing load characteristics were predicted within ten percent using the effective bearing clearance.

The spiral-groove double-acting hydrodynamic thrust bearing was subjected to thermally induced gradients to $67^{\circ}F$/inch radially, $240^{\circ}F$/inch axially, and $60^{\circ}F/\pi$ radians circumferentially. The effective bearing axial clearance after accounting for bearing distortions as determined from statically measured axial end play readings agreed within five percent of the clearance required to produce the measured dynamic characteristics. This verifies the results obtained during mechanical distortion evaluations and indicates that thrust bearing performance can be predicted once the type of distortions within the bearing is known.

REFERENCES

1. Lewis, P. Eusepi, M.W. and Wilson, D., "Research on Gas Lubrication at High Temperatures and Low Flow Rates," APL-TDR-46-56, Part III, April 1966. Contract AF-33(657)-10694.

2. Wilson, D., Murray, F., "Gas Lubrication Research for 1900 F Non-isothermal Operation," AFAPL-TR-67-57, Part I, May 1957. Contract AF-33(615)-3235.

3. Eusepi, M, Wilson, D. and Murray, F., "Gas Lubrication Research for 1900 F Non-isothermal Operation," AFAPL-TR-67-57, Part II, July 1968, Contract AF-33(615)-3235.